

Part I. Decrepitation and degassing behaviour of quartz up to 1560 °C: Analysis of noble gases and halogens in complex fluid inclusion assemblages

M.A. Kendrick *, D. Phillips, J.McL. Miller

Predictive Mineral Discovery CRC, School of Earth Sciences, University of Melbourne, Vic. 3010, Australia

Received 7 February 2005; accepted in revised form 22 December 2005

Abstract

Stepped heating and crushing experiments have been used to investigate the noble gas and halogen degassing behaviour of quartz in detail. Samples with diverse character were selected from the Eloise and Osborne, Iron Oxide Copper Gold (IOCG) ore deposits, and the Railway Fault, 13 km south of the Mt Isa Mine, in the Proterozoic Mt Isa Inlier of northeast Australia. Quartz has been shown to have a bimodal degassing profile. The first degassing mode at temperatures of <700 °C is caused by thermally induced mechanical decrepitation of fluid inclusions. Changes in the Br/Cl, I/Cl, Ar/Cl and $^{40}\text{Ar}/^{36}\text{Ar}$ composition of gas released at different temperatures up to 700 °C can be related to the decrepitation of different types of fluid inclusion observed by microthermometry. These variations with temperature permit deconvolution of the complex fluid inclusion assemblages associated with the IOCG samples; the ultra high salinity, multi solid (MS) and liquid–vapour–daughter (LVD) fluid inclusions, with a predominantly primary origin, decrepitate at higher temperatures than lower salinity liquid–vapour (LV) and monophasic (M) fluid inclusions that have a predominantly secondary origin. Three of the IOCG samples have primary MS and LVD fluid inclusions characterized by molar Br/Cl values of between 0.25×10^{-3} and 0.66×10^{-3} , I/Cl between 0.37×10^{-6} and 5.0×10^{-6} , $^{40}\text{Ar}/^{36}\text{Ar}$ values of <1000 and low ^{36}Ar concentrations of $0.7\text{--}1.0 \times 10^{-6} \text{ cm}^3 \text{ cm}^{-3} \text{ H}_2\text{O}$. These low values are most easily explained by the involvement of halite dissolution water in IOCG genesis. One of the IOCG samples has Br/Cl of $1.3\text{--}2.0 \times 10^{-3}$ and I/Cl of 10×10^{-6} , similar to juvenile magmatic fluids in Phanerozoic Porphyry Copper Deposits. This sample also has a higher ^{36}Ar concentration of $3.5 \times 10^{-6} \text{ cm}^3 \text{ cm}^{-3} \text{ H}_2\text{O}$ and a slightly elevated $^{40}\text{Ar}/^{36}\text{Ar}$ of 2236. Step heating reveals limited and non-systematic variation within the more homogenous population of LV fluid inclusions from the Railway Fault. The samples have mean values of 8.1×10^{-3} for Br/Cl; $9.4\text{--}12 \times 10^{-6}$ for I/Cl; <2000 for $^{40}\text{Ar}/^{36}\text{Ar}$; and $4.7\text{--}4.8 \times 10^{-6} \text{ cm}^3 \text{ cm}^{-3} \text{ H}_2\text{O}$ for ^{36}Ar concentration. The Br/Cl values are similar to those previously reported for basinal brines present in silicic alteration at the Mt Isa Mine and the additional data can be explained by interaction of such a bittern brine with fine grained sedimentary rocks in the sub-surface. The second mode of quartz degassing occurs between 1200 and 1450 °C and releases a greater volume of gas than the first degassing mode. Several lines of evidence, including microscope observations, indicate that the gas released at high temperature is also from the fluid inclusion reservoir. However, its release may be triggered by a metastable phase transition of quartz (~1200 °C) and caution is required in interpretation of the fluid compositions obtained at these temperatures. The data provide an improved understanding of fluid inclusion decrepitation behaviour that is different to that obtained in lower temperatures experiments designed by other workers to investigate H-isotope fractionation.

© 2006 Elsevier Inc. All rights reserved.

1. Introduction

Simultaneous analysis of fluid inclusion noble gas and halogen compositions by extended Ar–Ar methodology

(neutron irradiation and noble gas mass spectrometry) has been demonstrated as a powerful technique for unravelling the origin of hydrothermal fluids in Phanerozoic ore deposits from a variety of tectonic settings (e.g., Böhlke and Irwin, 1992a,b; Turner et al., 1993; Irwin and Roedder, 1995; Kendrick et al., 2001a,b, 2002a,b, 2005). The fluid Br/Cl value is widely regarded as behaving conservatively

* Corresponding author. Fax: +61 3 8344 7761.

E-mail address: mark.kendrick@unimelb.edu.au (M.A. Kendrick).

in the Earth's crust and characteristic values indicate different fluid origins. Similarly, the noble gases are inert elements and have isotopic compositions that vary by orders of magnitude between the crust or mantle, and the modern hydrosphere or atmosphere (e.g., Ballentine et al., 2002).

The technique is advantageous because the high sensitivity of noble gas mass spectrometers to noble gas isotopes allows the determination of Cl, Br, I, K, Ca, and U in very small sample sizes from irradiation-produced nucleogenic noble gas isotopes: $^{38}\text{Ar}_{\text{Cl}}$, $^{80}\text{Kr}_{\text{Br}}$, $^{128}\text{Xe}_{\text{I}}$, $^{39}\text{Ar}_{\text{K}}$, $^{37}\text{Ar}_{\text{Ca}}$, and $^{134}\text{Xe}_{\text{U}}$. Furthermore, fluid inclusion noble gas concentrations can be obtained from thermometric salinity measurements and the Ar/Cl ratio (Kelley et al., 1986; Turner and Bannon, 1992). When coupled with laser ablation, analysis of small groups of fluid inclusion is possible (Böhlke and Irwin, 1992c; Irwin and Roedder, 1995; Kendrick et al., 2001a). However, simultaneous measurement of the naturally occurring noble gas isotopes of Ar, Kr, and Xe is more easily attained in thick section sized samples of 10's of mg (Kendrick et al., 2001a). In some circumstances, Ar–Ar age information can be obtained from either the fluid inclusions or other impurities within the quartz (Kelley et al., 1986; Turner and Bannon, 1992; Kendrick et al., 2001a; but see Kendrick et al., 2006).

In the present contribution, we explore the potential for stepped heating to resolve different types of fluid inclusion hosted by quartz. This approach does not have the spatial resolution of laser ablation but seeks to exploit the different decrepitation temperatures of specific fluid inclusion types within complex fluid inclusion assemblages. It has the potential advantage that a population of fluid inclusions can be characterised rapidly. It is advantageous over in vacuo crushing because $^{38}\text{Ar}_{\text{Cl}}$ retention in daughter minerals (Kendrick et al., 2001a) is minimized by daughter mineral dissolution during the heating cycle.

The stepped heating experiments continue to temperatures of 1560 °C and together with limited crushing experiments provide insight into the siting of the noble gases, halogens and K within quartz samples. Understanding the distribution of impurities between grain boundaries, micron-sized fluid inclusions, mineral impurities or the quartz matrix (either nanometre-sized defects, substitutions for Si^{4+} or channels parallel to the *c*-axis), is critical to understanding geochemical data (e.g., Barker and Robinson, 1984; Ihinger and Zink, 2000; Grant et al., 2003; Watson and Cherniak, 2003; Götze et al., 2004).

The focus of this study (Part I) is on understanding the degassing behaviour of quartz and demonstrating that stepped heating experiments can be related to fluid inclusion decrepitation temperatures. The Ar–Ar systematics of the samples are examined in further detail in Part II (Kendrick et al., 2006). The study is of additional interest because it represents the first application of the combined noble gas and halogen technique to Proterozoic ore deposits and is the first on Australian localities.

2. Samples and microthermometry

Four quartz vein samples were selected from the Eloise (1530 Ma; Baker et al., 2001) and Osborne (1595 Ma; Gauthier et al., 2001) Iron-Oxide–Copper–Gold (IOCG) deposits of the Eastern Succession of the Proterozoic Mt Isa Inlier, northeast Australia (Fig. 1). An additional sample was obtained from the Railway Fault, 13 km south of the Mt Isa Copper Mine, in the Western Succession.

Detailed microthermometry has been reported previously for the Eloise samples (Baker, 1998). It is duplicated here for the sample splits analysed and for the Osborne and Railway Fault samples. However, additional emphasis was placed on determination of the fluid inclusion decrepitation temperatures. This was achieved by mapping the positions of 5–15 selected primary, pseudo-secondary and secondary fluid inclusions in several $\sim 1\text{ mm}^2$ wafer fragments and then recording the temperatures of vapour disappearance, daughter mineral dissolution, and decrepitation during a single heating cycle to 600 °C. A heating rate of 10 °C min^{-1} was used for this purpose giving an estimated accuracy of $\pm 10\text{ °C}$.

2.1. Eloise and Osborne fluid inclusion types

The IOCG samples from Eloise and Osborne include five different types of primary and secondary fluid inclusion with different relative abundances (Table 1). Both the primary and the secondary fluid inclusions have previously been attributed to stage II/III mineralization at Eloise (Baker, 1998) and the Ar–Ar systematics of the Osborne samples also suggest near synchronous formation of primary and secondary fluid inclusions (Kendrick et al., 2006). In order of decreasing salinity the types comprise:

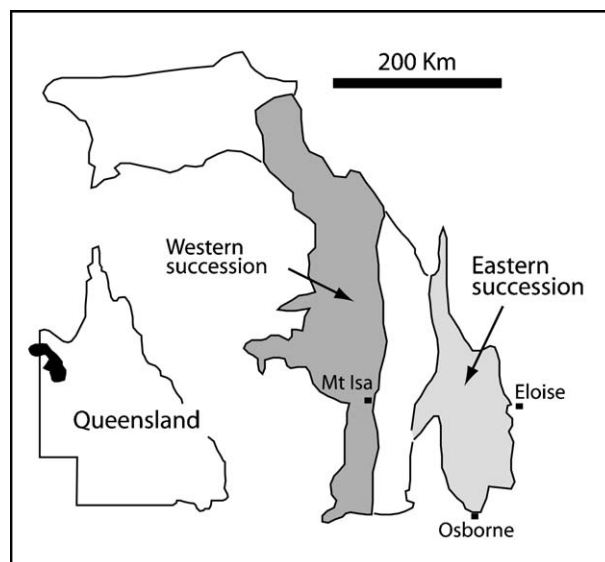


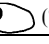
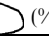



Fig. 1. Locality map indicating the position of the Mt Isa Inlier within western Queensland, northeast Australia, and the locations of Osborne, Eloise and Mt Isa.

Table 1
Fluid inclusion relative abundance

Sample	Primary (%)	MS  (%)	LVD  (%)	LV  (%)	M  (%)	CO ₂  (%)	Cap.Mica
<i>Eloise</i>							
EL 48177	<20	2–15	30–60	10–15	0	10–20	No
EL 48179	<10	0–2	10–40	50–60	5–20	10–20	No
<i>Osborne</i>							
OS37A	<10	2–4	10–25	40–60	0	15–20	?
OS 37B	<50	20–60	10–30	20–40	0–15	5–20	No
<i>Railway Fault</i>							
AWO2-002	100	0	0	100	0	0	Yes

Primary, maximum proportion of pseudo-secondary and isolated fluid inclusions considered to have a primary origin; MS, multisolid fluid inclusions; liquid, vapour, halite + 1 or more other daughter minerals; LVD, liquid–vapour and halite; LV, liquid–vapour; M, monophasic; CO₂, liquid carbon dioxide fluid inclusions.

(1) Ultra high salinity multi-solid (MS) fluid inclusions with up to five daughter minerals that usually have a primary origin. During heating, vapour disappearance occurred before daughter mineral dissolution at 80–200 °C, sylvite was the first salt to dissolve and the halite cube remained to between 400 and ~500 °C. Carbonate and unidentified daughter minerals, that probably include pyrosmalite [(Fe,Mn)₈Si₆O₁₅(OH,Cl)₁₅] or Fe-chloride (Baker, 1998), sometimes remained undissolved at 600 °C or at the point of decrepitation. Based on the NaCl–H₂O system these fluid inclusions have salinities of at least 40–65 wt%.

(2) High salinity liquid–vapour–daughter (LVD) fluid inclusions in which halite is the only daughter mineral are present as both primary and pseudosecondary as well as secondary fluid inclusions. Vapour disappearance occurred between 80 and 200 °C before halite dissolution which usually occurred between 100 and 300 °C but occasionally at ~400 °C, indicating salinities of 26–45 wt%. Complete homogenisation occurred before decrepitation.

(3) Liquid–vapour (LV) fluid inclusions are predominantly on trails indicating a secondary or pseudosecondary origin. They have first melting temperatures as low as –50 °C indicating a Ca-rich composition, meaning that salinities expressed as wt% NaCl eq. are overestimated. Final melting occurred between –44 and –5 °C

suggesting variable salinity of approximately 5–26 wt%. Vapour disappearance occurred over a similar interval to the MS and LVD fluid inclusions, between 80 and 200 °C.




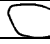

(4 and 5) Monophasic (M) and carbon dioxide (CO₂) fluid inclusions are predominantly on trails indicating a secondary origin.

The mean decrepitation temperatures are slightly different for each of the samples, but in general, LV fluid inclusions decrepitate at lower temperatures than LVD fluid inclusions and, where present, MS fluid inclusions decrepitate at the highest temperatures or remained undecrepitated by 600 °C (Table 2). Most CO₂ fluid inclusions remain undecrepitated at 600 °C, but some decrepitate around ~400 °C.

2.2. Railway Fault fluid inclusions

Primary LV fluid inclusions define growth zones in sample AW02-002 from the Railway Fault. This sample is included because accidentally trapped mica present within the fluid inclusions represents the major K reservoir, and enables us to evaluate the effect mica impurities have on Ar outgassing and Ar–Ar age determination (see also, Part II; Kendrick et al., 2006).

Table 2
Decrepitation temperatures °C

Sample	<i>n</i>	MS 		LVD 		LV 		M 		CO ₂ 
<i>Eloise</i>										
EL 48177	26	>600	510 to >600	418	340–450	515	340 to >600	295	250–340	>600
EL 48179	22			511	428–580	392	300–530			>600
<i>Osborne</i>										
OS 37A	59	437	390 to >600	415	240–590	412	340–485	415	410–420	>600
OS 37B	39	543	450 to >600	481	390 to >600	437	240–560			>600
<i>Railway Fault</i>										
AW02-002	26					~400	300–600			

n, number of decrepitation measurements for the sample. The mean decrepitation temperature and the range of decrepitation temperatures is given for each fluid inclusion type for which there are measurements.

The LV fluid inclusions have variable degrees of fill, between 10 and 90%, and final melting occurred in two modes. Most fluid inclusions have final melting temperatures of between -3 and -15 °C with a mean value of -8 °C. This indicates a mean salinity of ~ 12 wt% NaCl eq., but first melting occurred at -35 and -27 °C in two fluid inclusions suggesting Ca^{2+} in addition to Na^{+} and therefore that 12 wt% is an upper limit on salinity. A minor group of fluid inclusions had final melting temperatures between -0.5 and 0 °C indicating negligible salinity. Homogenisation temperatures varied between 160 and 380 °C, however, some of the highest values may result from necking down or leakage. The highest homogenisation temperature observed concurrently in several fluid inclusions of the same growth zone was 300 °C. Significant numbers of fluid inclusions began to decrepitate at ~ 300 °C and continued to do so up to 600 °C. The wafer could be seen to 'twitch' around 400 °C when the greatest number of fluid inclusions were decrepitating.

These data indicate considerable inter growth zone variability in T_h and T_m but the ranges are similar to those reported within silicic alteration at the Mt Isa Mine (Heinrich et al., 1989). The sense of movement, strike direction and relative age of the Railway Fault together with the high Cu-content of fluid inclusions in this sample have previously been used to suggest a link with Cu mineralization (~ 1523 Ma; Perkins et al., 1999) at the Mt Isa mine (A. Wilde, Pers. Comm. 2005).

3. Noble gas and halogen methodology

3.1. Sample preparation and irradiation

High purity quartz separates were obtained by crushing the off-cuts, from the thick sections used for microthermometry, and hand picking under a binocular microscope. The quartz chips were cleaned in an ultrasonic bath using distilled water and acetone and the cleaned chips were wrapped in Al-foil and packed into a silica glass tube.

The packed samples were irradiated for 150 MWH in position 5c of the McMaster University nuclear reactor, Canada (Irradiation designated UM#4). The neutron fluence was monitored using the Hb3Gr (1072 Ma) and GA1550 (98.8 Ma) irradiation monitors. J values were obtained from both monitors, while the additional β and α parameters were obtained from Hb3Gr alone (Appendix A; Kelley et al., 1986). J and β were used to calculate the fluence of fast and thermal neutrons (together approximately 10^{19} neutrons cm^{-2}), and thus to determine the abundance of Ca, Cl, and K measured as $^{37}\text{Ar}_{\text{Ca}}$, $^{38}\text{Ar}_{\text{Cl}}$, and $^{39}\text{Ar}_{\text{K}}$, respectively. Ar-isotopes were corrected for mass discrimination, ^{37}Ar and ^{36}Cl (producing ^{36}Ar) decay after irradiation, and other Ar-interference-reactions based on irradiated pure CaF_2 and K_2SO_4 . Ca was determined for this purpose, but because it has a low abundance and elevated uncertainty and was not detected in every step, it is not reported.

The Br/Cl and I/Cl values are proportional to the measured $^{80}\text{Kr}_{\text{Br}}/^{38}\text{Ar}_{\text{Cl}}$ and $^{128}\text{Xe}_{\text{I}}/^{38}\text{Ar}_{\text{Cl}}$ values (Appendix A). The minimum analytical uncertainty is determined by the reproducibility of atmospheric Kr/Ar and Xe/Ar values over the period of analysis. At the 1 sigma level these were 1.5–3% and 3–5% respectively, compared to 0.1–0.2% for the $^{40}\text{Ar}/^{36}\text{Ar}$ value. However, uncertainty is increased in very low gas volume extraction steps and the absolute uncertainty is determined by the relative fluxes of resonant and thermal neutrons. A suitable monitor for resonant neutrons was not available at the time of irradiation, but three sample duplicates have been included in a fully monitored irradiation that included the Shallowater meteorite (I–Xe) standard and confirm that the resonance correction is similar to previous irradiations. The calculated Br/Cl plus I/Cl values are reduced by factors of 1.3 and 1.7, respectively, when resonance is taken into account (Johnson et al., 2000; Kendrick et al., 2001ab; 2002a; 2005a), the resulting uncertainty in Br/Cl and I/Cl is estimated at 10%.

3.2. Gas extraction and analysis

Following irradiation, 20–130 mg of quartz chips were loaded in Cu-foil packets and placed in a vacuum sample chamber coupled to a tantalum-resistance-furnace and MAP 215-50 mass spectrometer at the University of Melbourne. Smaller quantities (20–50 mg) of samples AW02-002b and EL 48177 were also loaded into modified nupro® valves for in vacuo crushing; in these cases the crushed residue was later loaded in Cu-foil packets and the resistance furnace, as above.

The extraction line and loaded samples were baked at a temperature of ~ 120 °C to remove absorbed atmosphere and achieve UHV. Care was taken not to exceed 130 °C so as to avoid premature decrepitation of fluid inclusions although slightly higher temperatures may have been attained during sample irradiation.

Each sample was cyclically heated in a stepwise fashion from an idle temperature of 100 °C up to a maximum of 1560 °C. The temperature selected for each step was determined by the volume of gas measured in the previous step and varies for each sample (Appendix B). Heating to the desired step temperature was achieved over 3 min and each step had a duration of 20 min. Stepwise in vacuo crushing comprised 3–6 crushes.

Extracted gases were expanded into the extraction line, isolated from the cooling furnace, and purified over a period of 15 min using one hot and one cold Zr–Al getter (SAES st101). The purified noble gases (Ar, Kr, and Xe) were then admitted to the mass spectrometer and isotopically analysed sequentially over a period of 50 min with nine complete cycles of measurement. Ar isotopes were measured using a Faraday detector while Kr and Xe isotopes were analysed at a relative gain of ~ 400 using a Johnson electron multiplier.

3.3. Instrument blanks

Instrument blanks for stepwise heating were close to the Faraday detection limit of 10^{-12} cm⁻³ STP for ³⁶Ar, ³⁷Ar, ³⁸Ar, and ³⁹Ar and accounted for between 1% and 10% of the total ⁴⁰Ar gas released by a typical sample. The blanks increased by up to four times at high temperature and, where ³⁶Ar was detected, had an atmospheric ⁴⁰Ar/³⁶Ar composition. In all cases, the halogen derived noble gas isotopes, ⁸⁰Kr_{Br} and ¹²⁸Xe_I, had a blank level of <10% and in many cases <1% of sample gas. The atmospheric ⁸⁴Kr and ¹²⁹Xe instrument blanks were not detectable or close to the multiplier detection limit (2.7 and 2.2×10^{-15} cm⁻³ STP, for Kr and Xe, respectively). However, it was found that the empty Cu-foil capsule made a significant contribution to the ⁸⁴Kr and ¹²⁹Xe blank at temperatures of <600 °C. Although, believed to represent absorbed atmosphere this component was preferentially enriched in the heavier noble gases Xe > Kr > Ar meaning that the ⁸⁴Kr/³⁶Ar and ¹²⁹Xe/³⁶Ar ratios determined at <600 °C are unreliable and are not reported.

Instrument blanks for in vacuo crushing were lower than cold furnace blanks. Only ⁴⁰Ar was significantly above the Faraday detection limit, but due to the large volume of gas released by in vacuo crushing, this accounted for as little as 0.1–1%, exceptionally reaching 5%, of the sample gas. Kr and Xe isotopes are below or very close to the multiplier detection limit. Where measured, ⁸⁴Kr accounts for <1% of the typical sample gas and is presumed to have an atmospheric origin. Sample gas abundance data are reported in Appendix B.

4. Sample degassing

4.1. Degassing profiles

The degassing behaviour of quartz was examined in detail by stepped heating samples from Eloise, Osborne and the Railway Fault in 9–26 increments. All of the samples behaved in a consistent manner similar to samples previously reported from the UK (Kelley et al., 1986), suggesting that the profiles presented in Fig. 2 are typical for quartz. Sample AW02-002, which includes accidentally trapped mica, was analysed in the most detail and is emphasised throughout this section.

Chlorine-derived ³⁸Ar_{Cl} was degassed bimodally from each sample. Approximately 26% of the ³⁸Ar_{Cl} was released from sample AW02-002a during the low temperature degassing peak (L <700 °C), 62% was released during the high temperature peak (H ~1200–1450 °C) and only 6% was released in the intervening temperature interval (Table 3; Appendix B). The low temperature peak corresponds with a dewatering peak, previously reported for unrelated quartz (Barker and Robinson, 1984; Fig. 2a), but the relationship of the high temperature peak to dewatering is unclear because of the lack of dewatering data at high temperature.

In sample AW02-002b, analysed by combined in vacuo crushing and stepped heating, 58% of ³⁸Ar_{Cl} was released by crushing, compared to only 20% released during stepped heating of the uncrushed sample at <700 °C (Table 3). Crushing reduced approximately two thirds of the sample to a grain size of <90 µm, but left sufficient coarse material that many fluid inclusions could have remained intact (Fig. 3). During stepped heating of the crushed residue both the high and low temperature peaks were similarly reduced in size (Fig. 2b). Together these observations suggest that ³⁸Ar_{Cl} released in both the low and high temperature degassing peaks has a common origin in fluid inclusions.

The degassing profile of ³⁶Ar_{atm} is similar to ³⁸Ar_{Cl} indicating that most ³⁶Ar_{atm} is also contained in fluid inclusions, the small differences are explained by variable Cl/³⁶Ar and the presence of adsorbed ³⁶Ar_{atm} introduced as a modern atmospheric contaminant. The interpretation that fluid inclusion gas is responsible for the high as well as the low temperature degassing peak is substantiated further by the ³⁶Ar_{atm} degassing profiles of an unirradiated powdered split of sample AW02-002. Unlike the crushed residue with a significant number of >90 µm grains (Fig. 3) the <20 µm powder is effectively free of fluid inclusions and the high temperature degassing peak is completely absent from this sample (Fig. 4).

The degassing profiles of excess ⁴⁰Ar_E¹ and potassium-derived ³⁹Ar_K are similar to the ³⁸Ar_{Cl} and ³⁶Ar_{atm} degassing profiles for samples EL 41877, EL 41879 and OS 37B (Figs. 5a, b, and d), implying that ⁴⁰Ar_E, ³⁶Ar_{atm}, K and Cl are all hosted by the fluid inclusions in these samples. The small variations in the profiles indicate fluids with different compositions are released at different temperatures. In samples AW02-002a and -b, ³⁹Ar_K outgassing is unrelated to outgassing of ⁴⁰Ar_E, ³⁶Ar_{atm} or ³⁸Ar_{Cl} and in this sample K is hosted predominantly within accidentally trapped mica that is present within the fluid inclusions as a discrete sub-reservoir (Figs. 5e and f). The poor correlation between ³⁹Ar_K and ⁴⁰Ar_E (or ³⁸Ar_{Cl}) in sample OS 37A (Fig. 5c) may also be explained by the presence of very minor mica impurities.

The degassing patterns of the nucleogenic and atmospheric Kr and Xe isotopes; ⁸⁰Kr_{Br}, ¹²⁸Xe_I, ⁸⁴Kr_{atm}, and ¹²⁹Xe_{atm}, are similar to nucleogenic ³⁸Ar_{Cl} and atmospheric ³⁶Ar_{atm}. This suggests that fluid inclusions are the dominant reservoir of all trapped noble gases and halogens in natural quartz (see also Watson and Cherniak, 2003). Mineral impurities can be a significant reservoir of K and radiogenic ⁴⁰Ar_R but the quartz matrix does not appear to be a significant host to either K, the halogens or the noble gases.

¹ ⁴⁰Ar_E = excess ⁴⁰Ar: ⁴⁰Ar not attributed to an atmospheric source (⁴⁰Ar_A = $296 \times ^{36}\text{Ar}_{\text{atm}}$) or produced within the sample by radiogenic decay of K since the time of trapping, ⁴⁰Ar_R. ⁴⁰Ar_E = ⁴⁰Ar_{total} – ⁴⁰Ar_A – ⁴⁰Ar_R.

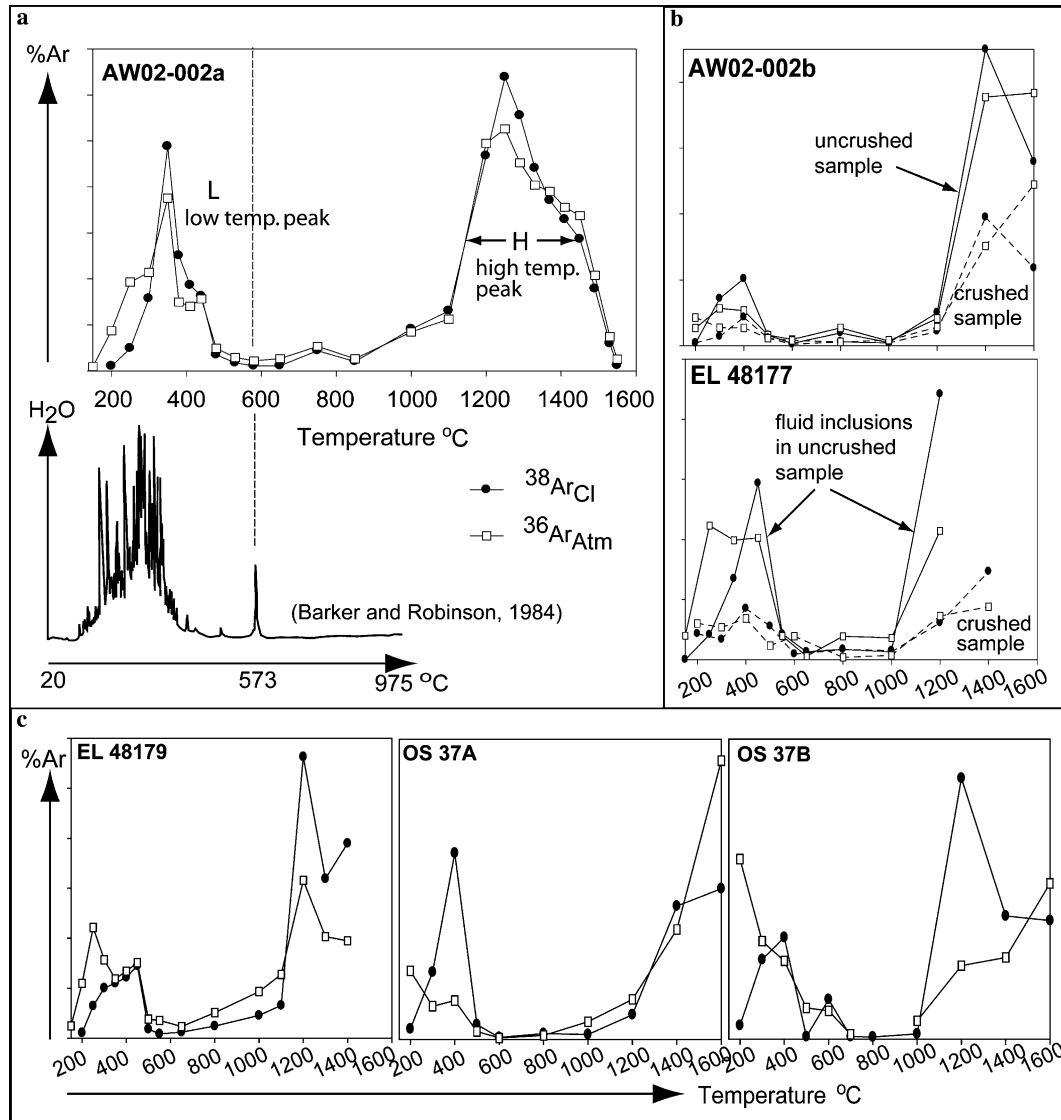


Fig. 2. Quartz degassing profiles for Cl-derived $^{38}\text{Ar}_{\text{Cl}}$ and atmospheric $^{36}\text{Ar}_{\text{atm}}$. (a) The highest resolution degassing profile (26 steps) for sample AW02-002a is compared with a previously published dewatering profile (Barker and Robinson, 1984). (b) The degassing profiles for crushed (dashed lines) and uncrushed (solid lines) splits of samples AW02-002b and EL 48177. (c) Degassing profiles for samples EL 48179, OS37B and OS37.

4.2. High temperature fractionation

The average Br/Cl and I/Cl values of inclusion fluids released during the low temperature ($<700^\circ\text{C}$) degassing peak are systematically higher than the Br/Cl and I/Cl values measured during the high temperature ($1200\text{--}1450^\circ\text{C}$) peak (Fig. 6; Table 3). However, this trend is not observed in samples that are crushed prior to stepped heating (Table 3). In contrast to the halogens, the initial $^{40}\text{Ar}/^{36}\text{Ar}$ values that have been corrected for post-entrapment production of radiogenic $^{40}\text{Ar}_{\text{R}}$, exhibit non-systematic variation between the low and high temperature degassing peaks (Fig. 6b).

In addition to the variation described above that is seen in all of the samples, sample AW02-002a studied in the most detail, exhibits a dramatic increase in both

F values² and the Br/Cl plus I/Cl values³ at temperatures of greater than $\sim 1450^\circ\text{C}$ (Fig. 7). Because both the F values and the Br/Cl plus I/Cl values are measured as Kr/Ar and Xe/Ar ratios, the sudden increase in all the values at $\sim 1450^\circ\text{C}$ indicates that the low volumes of gas released at the highest temperatures are enriched in the heavy noble gases on the order $\text{Xe} > \text{Kr} > \text{Ar}$. This effect cannot be ascribed to the instrument blank. The small volume of Ar released at this temperature was well above the blank level, and the volume of Kr and Xe

² F values = Fractionation values of atmospheric Xe or Kr relative to Ar. $F^{129}\text{Xe} = (^{129}\text{Xe}/^{36}\text{Ar})_{\text{sample}} / (^{129}\text{Xe}/^{36}\text{Ar})_{\text{air}}$; $F^{84}\text{Kr} = (^{84}\text{Kr}/^{36}\text{Ar})_{\text{sample}} / (^{84}\text{Kr}/^{36}\text{Ar})_{\text{air}}$.

³ Br/Cl is measured as $^{80}\text{Kr}_{\text{Br}}/^{38}\text{Ar}_{\text{Cl}}$ and I/Cl is measured as $^{128}\text{Xe}_{\text{I}}/^{38}\text{Ar}_{\text{Cl}}$.

Table 3
Noble gas and halogen degassing data

Sample	Crush or peak	$^{38}\text{Ar}/\text{Cl}$ (%)	$^{40}\text{Ar}/^{36}\text{Ar}$	Br/Cl ($\times 10^{-3}$)	I/Cl ($\times 10^{-6}$)
<i>Eloise</i>					
EL 48179	L	30	1331	0.72	2.3
	H	64	1472	0.34	1.5
EL 48177	L	?	1033	0.56	2.9
	H	?	1962	0.48	3.0
EL 48177	C	54	1012	0.88	2.9
	L	23	519	0.25	0.85
	H	21	1180	0.45	2.7
<i>Osborne</i>					
OS37A	L	?	514	1.5	17
	H	?	401	1.2	9.1
OS37B	L	32	374	0.58	3.6
	H	51	592	0.40	2.9
<i>Railway Fault</i>					
AW02-002a	L	28	1431	8.1	9.4
	H	62	2139	3.8	4.0
AW02-002b	L	20	1029	8.1	12
	H	50	706	6.5	4.1
AW02-002b	C	58	810	12	16
	L	8	421	6.1	11
	H	22	640	5.8	4.6

(1) L, gas extracted at <700 °C. H, gas extracted between 1200 and 1450 °C. C, gas extracted by in vacuo crushing.

(2) “?” question marks indicate samples incompletely outgassed at high temperature.

The measured $^{40}\text{Ar}/^{36}\text{Ar}$ values have been corrected for post-entrapment production of radiogenic $^{40}\text{Ar}_R$ based on K abundance and ages of 1530 Ma for Eloise (Baker et al., 2001), 1595 Ma for Osborne (Gauthier et al., 2001) and an assumed age of 1523 Ma for the Railway Fault.

released was many times greater than either the blank level or that released from the other samples at similar temperatures (Appendix B).

4.3. Fluid inclusion decrepitation

To better understand the degassing profiles described above, we highlight important aspects of the fluid inclusion decrepitation behaviour observed on the fluid inclusion stage (Tables 1 and 2), and the appearance of selected samples after heating to 1100 and 1400 °C in the tantalum resistance furnace.

On heating to 600 °C trails of secondary fluid inclusions were seen to ‘unzip’, with the largest fluid inclusions decrepitating first and the smallest fluid inclusions decrepitating at the highest temperature. Decrepitation of a given trail could proceed almost instantaneously or gradually over ~100 °C and different trails decrepitated at different temperatures. Sometimes a fluid inclusion was seen to leak before it decrepitated. The daughter minerals usually dissolved before the fluid inclusion decrepitated. However, in the most saline MS fluid inclusions, decrepitation frequently occurs before dissolution of the last one or two daughter minerals.

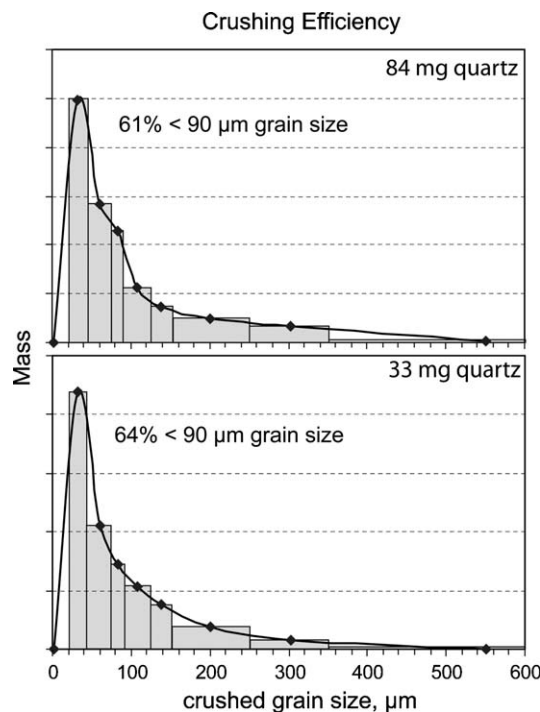


Fig. 3. Grainsize distribution plots for quartz samples crushed in modified nupro valves. The size fractions have been determined by sieving and are: <45 µm in size; 45–75; 75–90; 90–125; 125–150; 150–250; 250–354; and >354 µm. The area under the curve is equal to 100%. Crushing efficiency appears fairly independent of the quantity of sample crushed up to 84 mg.

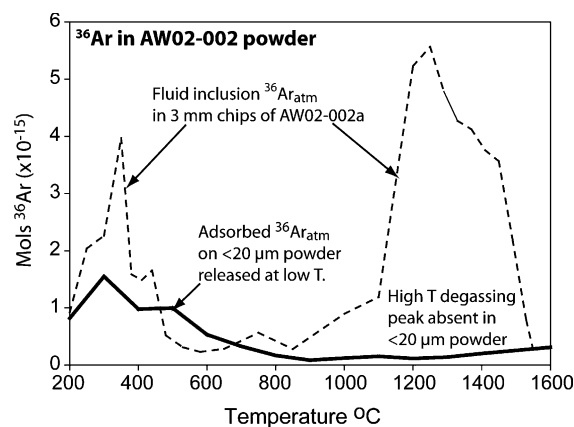


Fig. 4. Degassing profiles for ^{36}Ar from AW02-002 (126 mg before crushing, see also Fig. 2a) and 67 mg of powdered (1–20 µm) sample. The powder is much finer than achieved during in vacuo crushing (Fig. 3) and is effectively fluid inclusion free. To avoid handling difficulties the ground powder was not irradiated. As a consequence only the naturally occurring noble gas isotopes could be measured, because $^{40}\text{Ar}_R$ is present within a mica impurity in this sample, quartz degassing could only be monitored by $^{36}\text{Ar}_{\text{atm}}$. The presence of ^{36}Ar in the atmosphere and the fine grainsize of the sample meant that surface adsorption was significant, nonetheless it is clear that the high temperature degassing peak is now absent.

In all of the samples, heating to 600 °C appears to decrepitate the majority of fluid inclusions, but not all of them. However, it is virtually impossible to see into the smallest fluid inclusions of <2 µm and some of the decrepitated fluid inclusions may have only partially leaked. Fluid

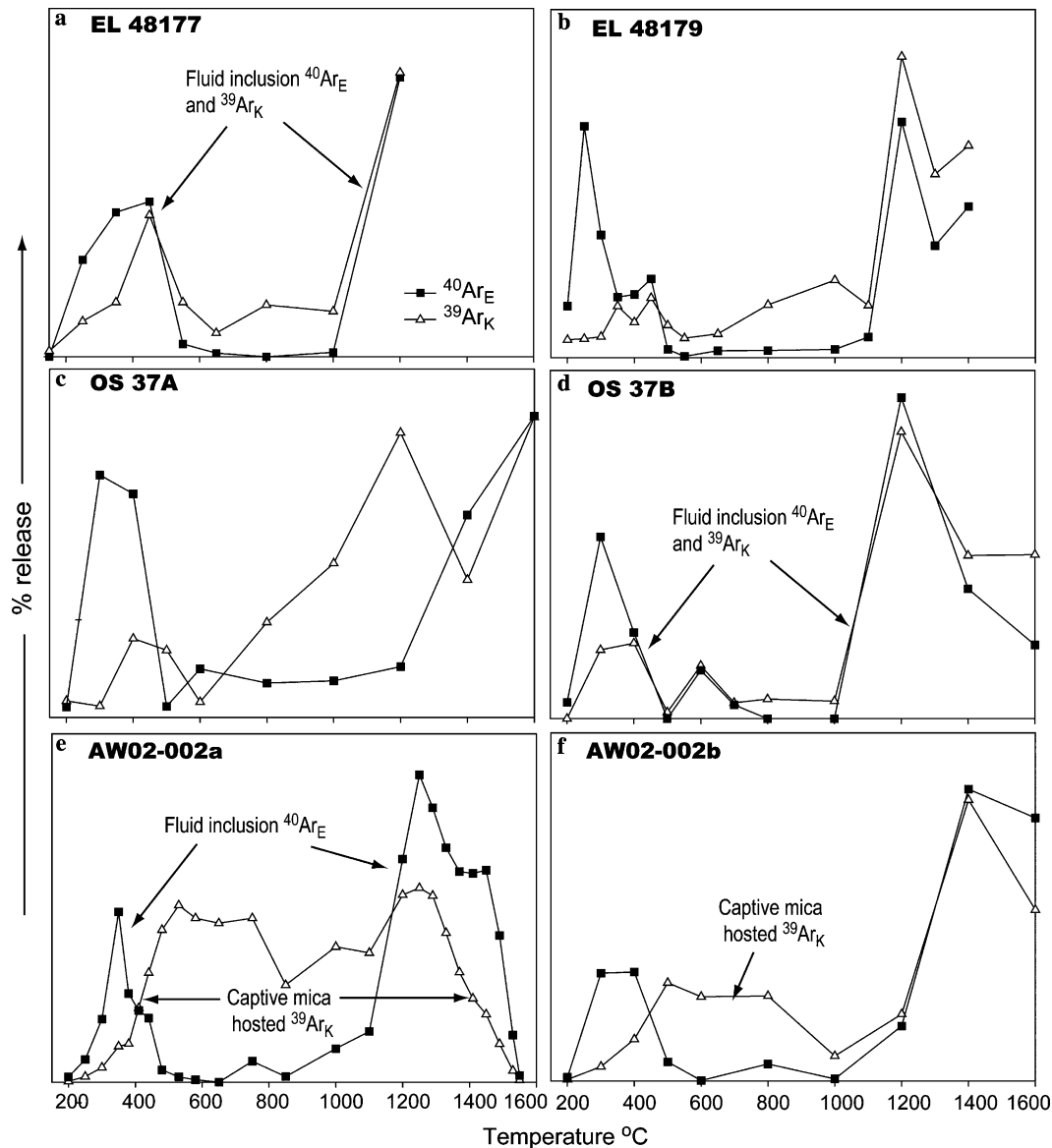


Fig. 5. Quartz degassing profiles for K-derived $^{39}\text{Ar}_\text{K}$ and excess $^{40}\text{Ar}_\text{E}$. (a and b) The Eloise samples have $^{39}\text{Ar}_\text{K}$ and $^{40}\text{Ar}_\text{E}$ degassing profiles consistent with an origin from fluid inclusions only (see also Fig. 2). (c) The $^{39}\text{Ar}_\text{K}$ and $^{40}\text{Ar}_\text{E}$ degassing profiles of sample OS 37A are poorly correlated. (d) Fluid inclusion degassing profiles for sample OS 37B. (e and f) Sample AW02-002 has a $^{40}\text{Ar}_\text{E}$ degassing profile similar to those of $^{38}\text{Ar}_\text{Cl}$ and $^{36}\text{Ar}_\text{atm}$ (see Fig. 2) consistent with an origin in the fluid inclusions, but K-derived $^{39}\text{Ar}_\text{K}$ has a unimodal degassing profile that is unrelated to fluid inclusion degassing. Nb- $^{40}\text{Ar}_\text{E}$ has been calculated from the measured ^{40}Ar and K and ages of 1530 Ma for Eloise, 1595 Ma for Osborne and 1523 Ma for the Railway Fault.

inclusion size as well as type is an important control on decrepitation temperature and the different fluid inclusion types exhibit considerable overlap in their decrepitation temperature (Table 2).

4.3.1. After heating to 1100 and 1400 °C

After heating to 1100 °C, before the second major degassing peak (Fig. 2), each of the samples retained a similar appearance to that attained after heating to only 600 °C on the fluid inclusion stage. Rare LV fluid inclusions can still be observed in samples OS 37A and AW02-002 (Figs. 9d and 10b). However, the majority of fluid inclusions appear to be vapour dominated and are either completely decrepitated or have partially leaked (Figs. 8–10).

After heating to 1400 °C, after the second major degassing peak (Fig. 2), the samples have a radically different appearance: micro-fracturing has affected samples EL 48179 (Figs. 8d and e) and AW02-002 (Fig. 10d). Explosive decrepitation has occurred in sample OS 37A and AW02-002, which results in 50–100 µm pits from which further fractures propagate (Figs. 9g and 10e). A vapour-dominated fluid inclusion remained intact and has a negative crystal shape in sample EL 48179 (Fig. 8f). However, most intriguingly, samples OS 37A, and AW02-002 have developed an entirely new radial fabric (Figs. 9f and 10f) and in sample OS 37A, a network of interconnected fluid inclusion ‘tubules’ that include a fluid phase (Fig. 10h). Although these textures have been observed in fluid inclusion wafers rather

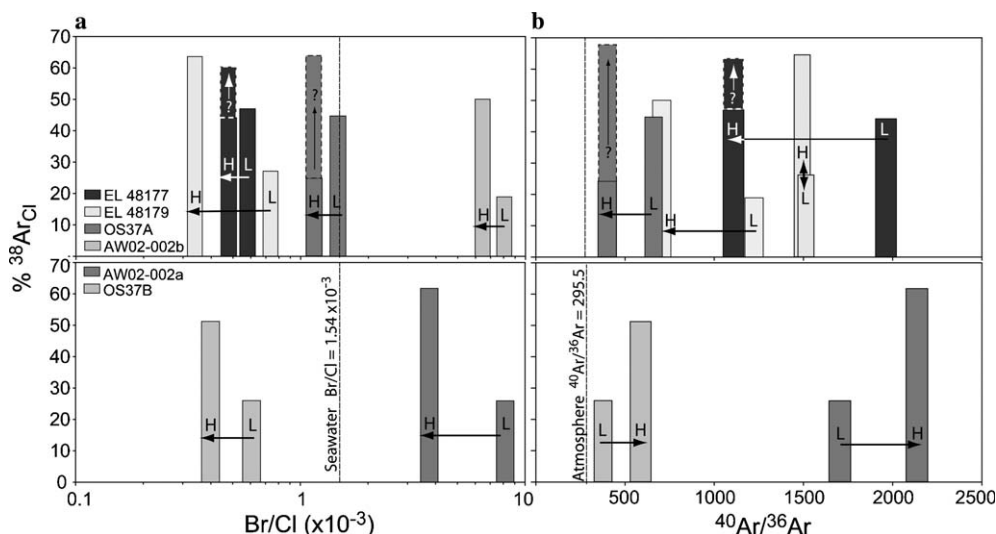


Fig. 6. Plots showing the composition of gas and the proportion of Cl-derived $^{38}\text{Ar}_{\text{Cl}}$ outgassed during the high (H; 1200–1450 °C) and low (L; <700 °C) temperature peaks of outgassing (see Fig. 2). (a) Br/Cl values of gas released at high temperature are systematically lower than at low temperature, the arrows indicate increasing temperature. A greater volume of gas is released during the high temperature peak than is released during the low temperature peak. (b) The initial $^{40}\text{Ar}/^{36}\text{Ar}$ value of gas released at high and low temperatures vary non-systematically. The initial $^{40}\text{Ar}/^{36}\text{Ar}$ values are corrected for post-entrapment production of radiogenic $^{40}\text{Ar}_{\text{R}}$. Nb-samples EL 48177 and OS37A were incompletely outgassed, the dashed boxes indicate an unknown volume of unmeasured gas.

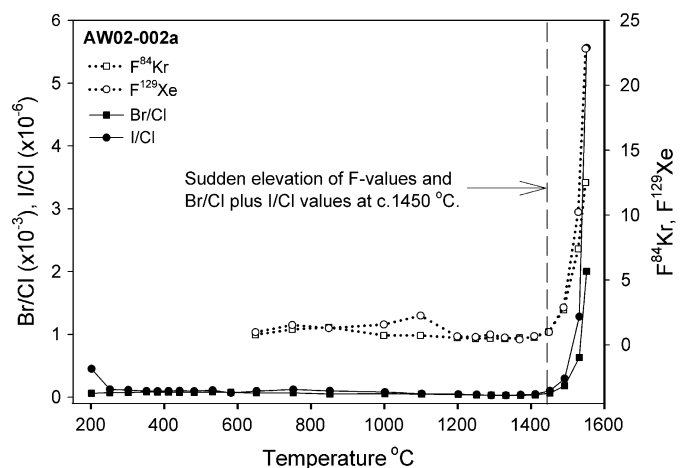


Fig. 7. Sample AW02-002a F values and apparent Br/Cl plus I/Cl values as a function of temperature. The apparent Br/Cl value at 1530 °C is geologically unrealistic. The sudden increase in all values at high temperature could be explained by either the preferential retention of $\text{Ar} > \text{Kr} > \text{Xe}$ in molten quartz or a diffusion related Rayleigh fractionation process, see text. The F values are noble gas fractionation values relative to air ($F_X = [X/^{36}\text{Ar}]/[X/^{36}\text{Ar}]_{\text{air}}$) and the Br/Cl plus I/Cl values are measured as $^{80}\text{Kr}_{\text{Br}}/^{38}\text{Ar}_{\text{Cl}}$ and $^{128}\text{Xe}_{\text{I}}/^{38}\text{Ar}_{\text{Cl}}$.

than the quartz chips used in the stepped heating experiments the degassing behaviour of wafers and chips is indistinguishable.

4.4. Interpretation of degassing profiles

The bimodal nature of the quartz degassing profile (Fig. 2) suggests that diffusion is not the primary control on the release of noble gases during stepped heating. Microscopic observations indicate that Ar-degassing from quartz at low temperature (<700 °C) is by the decrepitation of fluid inclusions. Although some fluid inclusions remain undecrepitated on the fluid inclusion stage by 600 °C, very little degassing occurs between 600 and 1200 °C (Fig. 2).

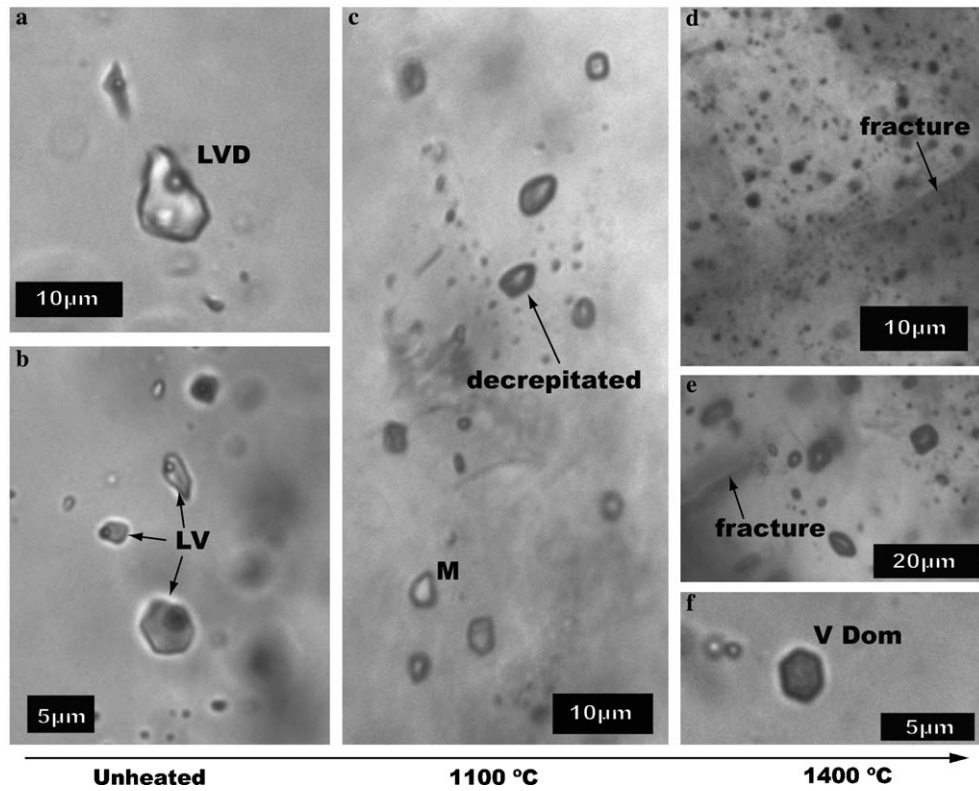
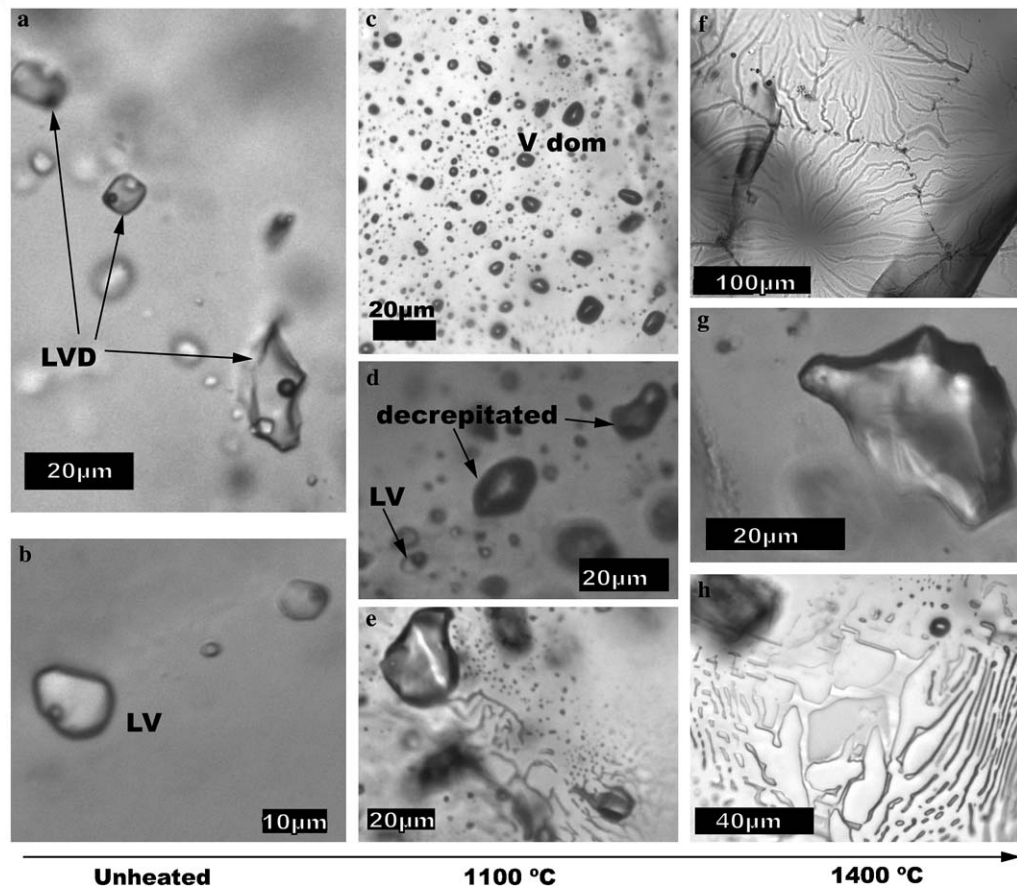
Five lines of evidence suggest that the gas released at high temperature (1200–1450 °C), is also from the fluid inclusion reservoir: (1) A fluid phase has been observed within quartz heated to 1400 °C (Fig. 9h). (2) Quartz heated to 1400 °C exhibits evidence for explosive decrepitation (Figs. 9g and 10e), while quartz heated to 1100 °C does not (Figs. 8–10). (3) More gas is released by crushing a sample than is released at <700 °C by stepped heating (Table 3). (4) Crushing a sample prior to step heating reduces the size of both the low and high temperature degassing peaks (Fig. 2b). (5) The high temperature degassing peak is absent in fluid inclusion free 20 μm powdered samples (Fig. 4).

4.4.1. Gas release triggers

It has previously been observed that the 573 °C phase transition of α -quartz to β -quartz promotes the decrepita-

Fig. 8. Photomicrographs of sample EL 48179 from Eloise. (a and b) Before heating. (c) After heating to 1100 °C in the UHV resistance furnace. (d–f) After heating to 1400 °C in the UHV resistance furnace. In the samples heated to 1100 °C vapour dominated fluid inclusions can be difficult to distinguish from those that have decrepitated. However, careful observation confirms many inclusions remain in tact.

Fig. 9. Photomicrographs of sample OS 37A from Osborne. (a and b) Before heating. (c–e) After heating to 1100 °C in the UHV resistance furnace. (f–h) After heating to 1400 °C in the UHV resistance furnace.

⑧ **EL 41879**⑨ **OS37A**

tion of fluid inclusions (Bodnar et al., 1989). Although our degassing curves are constructed from stepwise heating increments of 50–100 °C and do not have the resolution necessary to identify a degassing spike at 573 °C, a spike is seen at this temperature on the dewatering curve of Barker and Robinson (1984) (Fig. 2a). Barker and Robinson (1984) reported no further dewatering spikes, but their experiments did not reach temperatures of >1200 °C.

A phase transition is an attractive mechanism to explain the sudden degassing of our samples at ~1200 °C (Fig. 2). Impure fluid inclusion-rich natural-quartz under ultra-high-vacuum may behave quite differently to pure SiO₂ at 1 bar of pressure which transforms from β -quartz to tridymite at 867 °C and from tridymite to cristobalite at 1470 °C (Tuttle and Bowen, 1958). In particular, the temperature of metastable-melting or metastable-phase-transition is extremely sensitive to the rate of heating, particle size, surface conditions and the presence of gaseous, liquid or solid impurities (Hummel, 1984).

Possible phase transitions to explain the sudden release of gas at ~1200 °C include the tridymite-M to tridymite-S transition, or the metastable transition of superheated β -quartz to undercooled β -cristobalite (see Sosman, 1965 or Hummel, 1984). The metastable transition of superheated β -quartz to undercooled β -cristobalite (Fenner, 1913), is favoured because this would also explain the absence of any real dewatering spike at 867 °C (Fig. 2a; Barker and Robinson, 1984) and because the same phase diagram suggests metastable melting of β -cristobalite to undercooled liquid silica could occur at ~1450 °C (see Hummel, 1984).

The radial fabrics that are developed in samples OS 37A and AW02-002a, heated to 1400 °C (Figs. 9f and 10f), may be caused by volume changes associated with the proposed ~1200 °C phase transition. Furthermore, the change in the composition of noble gases released from sample AW02-002a at ~1450 °C (Fig. 7) could be explained by metastable melting of this sample leading to retention of Ar > Kr > Xe in the molten sample. The furnace crucible was empty after analysis of these samples, compatible with such an explanation. However, samples analysed more recently, with a new furnace liner, and fewer heating steps at high temperature, were not melted and did not exhibit the degassing pattern of sample AW02-002a, indicating that not all samples behave in the same way. Furthermore, the degassing pattern of this sample (Fig. 7), could alternatively be explained by a diffusion related Rayleigh fractionation process (see below).

4.5. Fluid inclusion analysis

Even though we have shown gases released at both low and high temperature are from fluid inclusions, only Br/Cl and I/Cl values measured at <700 °C, that can be related to the observed behaviour of decrepitating fluid inclusions (Table 2), are considered representative of the fluid inclusions composition.

The maximum temperature of 700 °C is selected to ensure that the total compositional variation within the entire low temperature degassing peak (Fig. 2) is determined, and because not all fluid inclusions have decrepitated at 600 °C (Table 2). A lower temperature of 300–500 °C has previously been suggested as most representative for δD values in quartz fluid inclusions (e.g., Ishiyama et al., 1999; Simon, 2001; Grant et al., 2003). The difference is explained because, unlike H, fluid inclusions are the only significant, reservoir for the noble gases and halogens in quartz. By contrast H is present within quartz as H₂O in fluid inclusions trapped as molecular H₂O; H₂O in nano-pores originally trapped as interstitial OH⁻; H⁺ or OH⁻ associated with Al³⁺ substitutions for Si⁴⁺; and neutrally charged LiOH molecules with uncertain speciation (Ishiyama et al., 1999; Ihinger and Zink, 2000; Simon, 2001; Grant et al., 2003).

The diverse H-reservoirs mean that heating schedules are designed to distinguish fluid inclusions from chemically distinct H-species in the quartz matrix and not between different types of fluid inclusion. The presence of three highly reactive or dipolar H-species, H₂O, OH⁻ and H⁺ (compared to inert mono-atomic gases) also means that H-isotope interpretation is complicated further by possible surface adsorption or H⁺ leakage (Mavrogenes and Bodnar, 1994; Simon, 2001). Our data suggest a further precautionary note, namely, it cannot be assumed that all H is released quantitatively from both fluid inclusion and matrix sites by thermal decrepitation of quartz at only 1100 or 1200 °C (Simon, 2001), rather significant fluid inclusions persist above 1200 °C.

We do not interpret the Br/Cl or I/Cl composition of inclusion fluids released at high temperature (1200–1450 °C) because two potential artefacts might contribute to the systematically different Br/Cl and I/Cl compositions measured at these temperatures.

- (1) Fluid inclusion decrepitation temperature is inversely proportional to size (Bodnar et al., 1989) and small fluid inclusions have been observed to remain preferentially undecrepitated at 600 °C. It is possible that very small fluid inclusions (or nano-pore crystal defects) include fluids with non-representative compositions (Roedder, 1984) and they could dominate the composition of fluids released at 1200–1450 °C. However, non-representative compositions in very small melt inclusions are caused by partitioning of elements along the grain boundary into the crystal matrix (Roedder, 1984). Therefore, it could be argued that the noble gas and halogen composition of fluid inclusions will probably be unaffected because neither noble gases or halogens are important constituents of quartz.
- (2) The role of diffusion is likely to become increasingly important at high temperature and could lead to preferential release of the lightest noble gases, on the order Ar > Kr > Xe. This would reduce the measured ⁸⁰Kr_{Br}/³⁸Ar_{Cl} and ¹²⁸Xe_I/³⁸Ar_{Cl} ratios giving low

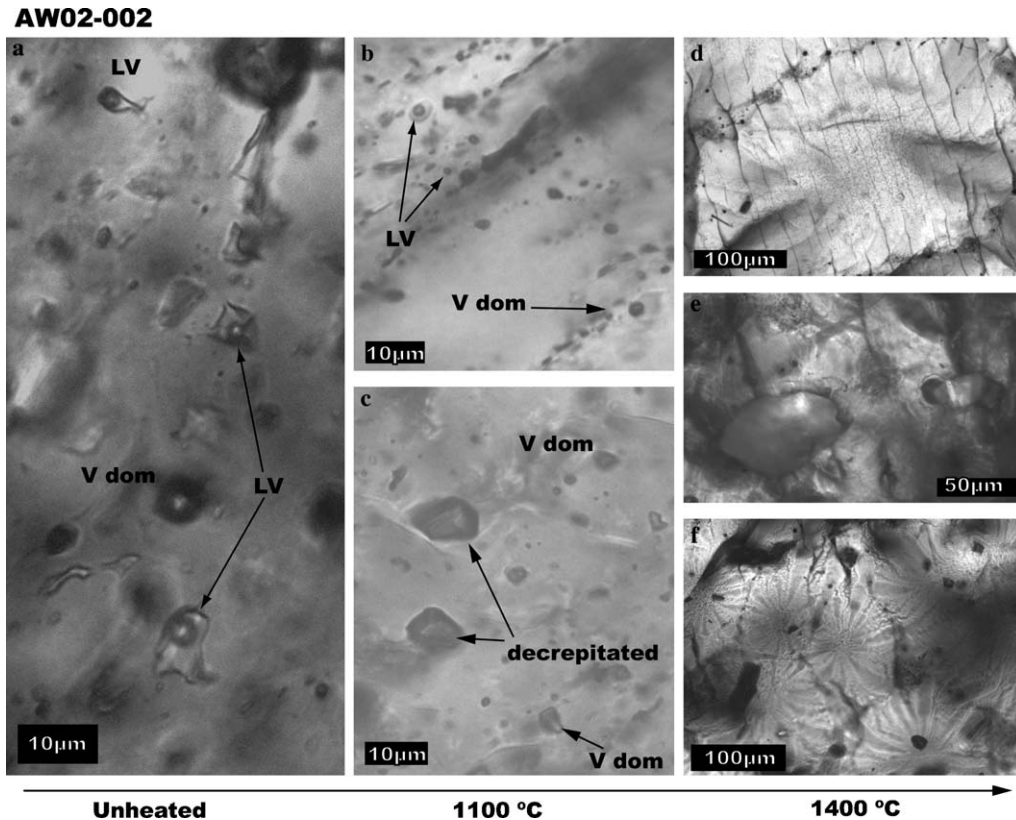


Fig. 10. Photomicrographs of sample AW02-002 from the Railway Fault. (a) Before heating. (b and c) After heating to 1100 °C in the UHV resistance furnace. (d–f) After heating to 1400 °C in the UHV resistance furnace.

Br/Cl and I/Cl values at high temperature, as observed. Such a mechanism would lead to preferential retention of the heavy noble gases in the quartz sample and a Rayleigh fractionation process could provide an alternative means to explain the elevated Br/Cl, I/Cl and F values measured in sample AW02-002a at >1450 °C (Fig. 7).

In contrast to the systematic difference in Br/Cl and I/Cl between the low and high temperature degassing peaks, the $^{40}\text{Ar}/^{36}\text{Ar}$ values exhibit non-systematic variation (Fig. 6b). The isotopes of Ar are very close in mass and size relative to Kr or Xe. It therefore seems that they are unaffected by the processes controlling the Br/Cl values. Consequently, the $^{40}\text{Ar}/^{36}\text{Ar}$ and Ar/Cl compositions measured at all temperatures are considered representative of the included fluids.

5. Noble gas and halogen geochemistry

5.1. Distinguishing primary and secondary fluid inclusions

The stepped heating data for the IOCG samples show considerable scatter on a $^{40}\text{Ar}/^{36}\text{Ar}$ versus $\text{Cl}/^{36}\text{Ar}$ diagram, with the $^{40}\text{Ar}_\text{E}/\text{Cl}$ values ranging between 10^{-4} and 10^{-6} (Fig. 11). High salinity primary fluid inclusions are expected to have the most elevated $\text{Cl}/^{36}\text{Ar}$ values.

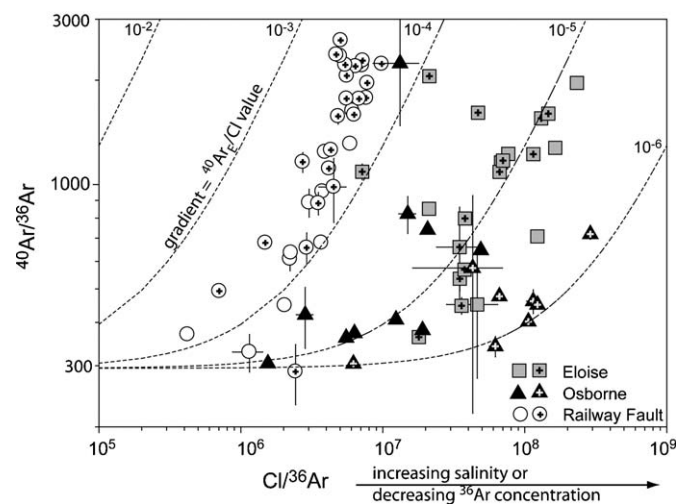


Fig. 11. Log-log plot of $^{40}\text{Ar}/^{36}\text{Ar}$ versus $\text{Cl}/^{36}\text{Ar}$. Eloise, empty square = EL 48177; crossed square = EL 48179; Osborne, empty triangle = OS 37A; crossed triangle = OS 37B; Railway Fault, empty circle = AW02-002b; crossed circle = AW02-002a. IOCG samples are poorly correlated, the spread in data reflects mixing between a high salinity high $\text{Cl}/^{36}\text{Ar}$ fluid, a lower salinity fluid with higher $^{40}\text{Ar}/^{36}\text{Ar}$ value and air with $^{40}\text{Ar}/^{36}\text{Ar} = 295$ and $\text{Cl}/^{36}\text{Ar} = 0$. Sample AW02-002 from the Railway Fault exhibits a more typical pattern with less spread in $^{40}\text{Ar}_\text{E}/\text{Cl}$. This is explained by mixing between a high salinity high $^{40}\text{Ar}/^{36}\text{Ar}$ fluid and a lower salinity fluid with lower $^{40}\text{Ar}/^{36}\text{Ar}$.

Therefore, the poor correlation between high $\text{Cl}/^{36}\text{Ar}$ and the highest $^{40}\text{Ar}/^{36}\text{Ar}$ values of slightly above 2000, indicate that extraction steps most representative of primary fluid inclusions do not have the highest $^{40}\text{Ar}/^{36}\text{Ar}$ values.

Compared to the IOCG samples, sample AW02-002 from the Railway Fault exhibits more typical behaviour in $^{40}\text{Ar}/^{36}\text{Ar}$ versus $\text{Cl}/^{36}\text{Ar}$ space, in that the data define a binary mixing array (Fig. 11). In this case the mixing array represents the two groups of primary LV fluid inclusions identified within the sample and has a mean $^{40}\text{Ar}_\text{E}/\text{Cl}$ value of $\sim 2 \times 10^{-4}$. The most saline fluid inclusions with a mean salinity of ~ 12 wt% NaCl eq. have $^{40}\text{Ar}/^{36}\text{Ar}$ values of < 3000 . The less saline group with final melting temperatures of close to zero have lower $^{40}\text{Ar}/^{36}\text{Ar}$ and $\text{Cl}/^{36}\text{Ar}$, although the lowest values may also have been affected by atmospheric contamination.

5.1.1. IOCG decrepitation profiles

$\text{Cl}/^{36}\text{Ar}$ values are highest in fluids that have the highest salinity or that have lost ^{36}Ar through devolatilisation. They are plotted as a function of temperature in Fig. 12a

and suggest that the highest salinity primary fluid inclusions dominate decrepitation release from EL 41879 and OS 37B at 400–450 °C and from EL 41877 and OS 37A at 600–650 °C. However, this conclusion is weakened by the possibility that atmospheric contamination has affected the extraction steps to different extents.

Atmospheric contamination is expected to be most significant at low temperature where adsorbed gases are first released from the samples' surface (Fig. 4). Despite this, the highest $^{40}\text{Ar}/^{36}\text{Ar}$ values are measured at low temperature in the Eloise samples and, as suggested, not in the same steps as the highest $\text{Cl}/^{36}\text{Ar}$ values (Figs. 12a and b).

The $^{40}\text{Ar}_\text{E}/\text{Cl}$ value is related to the $^{40}\text{Ar}/^{36}\text{Ar}$ and $\text{Cl}/^{36}\text{Ar}$ values (see Fig. 11), but because neither Cl or $^{40}\text{Ar}_\text{E}$ are present in the atmosphere, it is unaffected by atmospheric contamination. The lowest $^{40}\text{Ar}_\text{E}/\text{Cl}$ values correspond to fluids with the highest salinity or lowest $^{40}\text{Ar}_\text{E}$ concentration and were measured between 500 and 650 °C in the Eloise samples (Fig. 12c), but at lower temperature in the Osborne sample which has a high $^{40}\text{Ar}/^{36}\text{Ar}$ extraction step at 600 °C (Figs. 12b and c). Because the

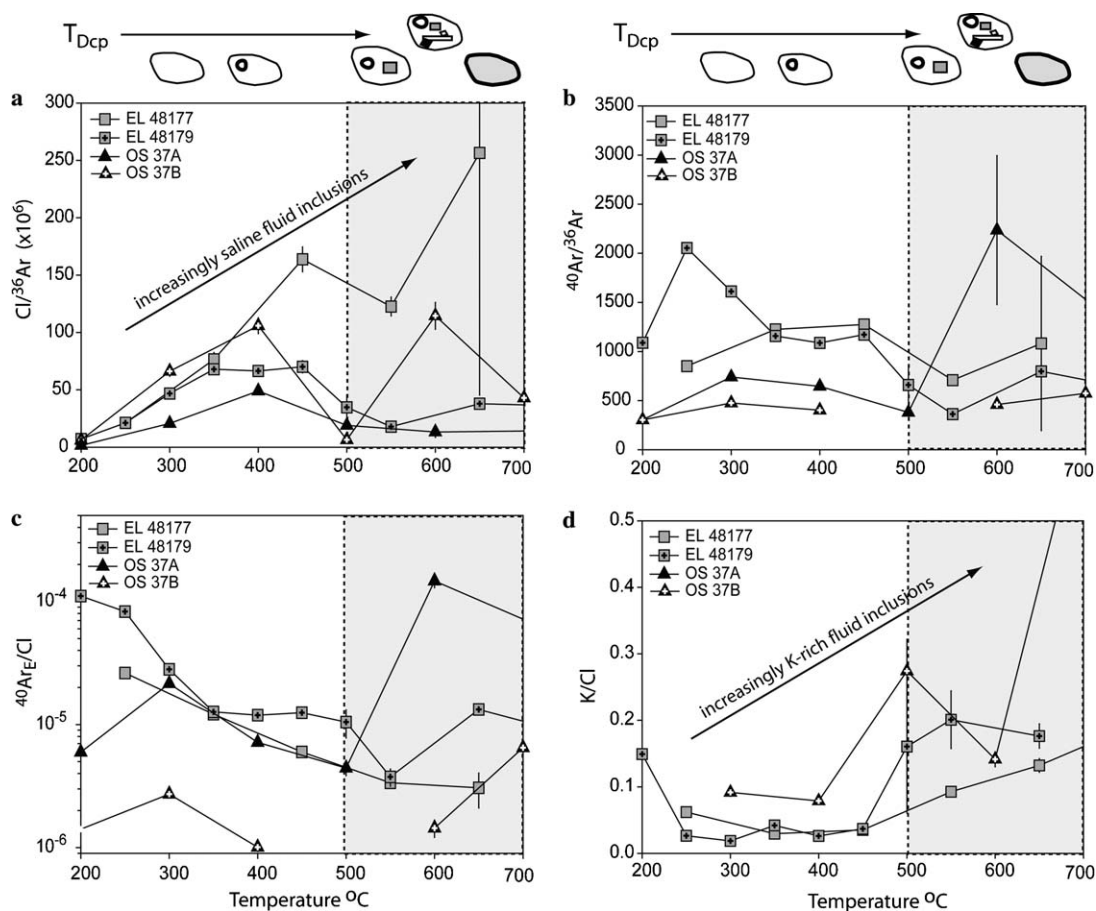


Fig. 12. Decrepitation profiles for the Eloise and Osborne IOCG deposits. The schematic above the plots indicate the microthermometry observation that the most saline LVD and MS fluid inclusions decrepitate at the highest temperatures of > 500 °C (see Table 2). (a) The highest $\text{Cl}/^{36}\text{Ar}$ values are measured at high temperature when the most saline primary fluid inclusions decrepitate. (b) The highest $^{40}\text{Ar}/^{36}\text{Ar}$ values are measured at low temperature in the samples from Eloise. With the exception of one data point Osborne exhibits little variation. (c) The lowest $^{40}\text{Ar}_\text{E}/\text{Cl}$ values are measured in the Eloise samples at high temperature, compatible with decrepitation of the highest salinity fluid inclusions. The high $^{40}\text{Ar}_\text{E}/\text{Cl}$ OS 37A data point at 600 °C corresponds with the high $^{40}\text{Ar}/^{36}\text{Ar}$ release from this sample. (d) The highest K/Cl values are measured at high temperature, suggesting K-rich multiphase inclusions decrepitate at this point.

variation in $^{40}\text{Ar}_\text{E}/\text{Cl}$ value cannot be explained by air contamination, this provides proof that stepped heating is sampling different fluid inclusion types at different temperatures.

The K/Cl values of both Eloise samples and OS 37B are highest at high temperature (Fig. 12d). The high K/Cl values of 0.15–0.3, that are measured at 500–700 °C in these samples, are realistic for K-rich MS primary fluid inclusions. Sample OS 37A has a K/Cl value of slightly greater than one at 600 °C, suggesting the presence of a very minor K-mineral impurity and it is omitted from Fig. 12d.

Measurement of the highest $\text{Cl}/^{36}\text{Ar}$, K/Cl values and lowest $^{40}\text{Ar}_\text{E}/\text{Cl}$ between 500 and 700 °C, supports the observation made during microthermometry that the highest salinity MS fluid inclusions decrepitate at the highest temperatures (Section 2.1).

Finally, the Br/Cl value is plotted as a function of temperature in Fig. 13. The IOCG samples have the lowest Br/Cl values between 500 and 700 °C which is interpreted as evidence that the highest salinity MS and LVD fluid inclusions have the lowest Br/Cl values (Fig. 13a). The Br/Cl values of sample AW02-002 from the Railway Fault exhibit less systematic variation with temperature, maximum Br/Cl values were measured at 350 and 550 °C in split-a and at 650 °C in split-b (Fig. 13b). The variation in this sample, that has a less variable $^{40}\text{Ar}_\text{E}/\text{Cl}$ value (Fig. 11), is interpreted to reflect variation in primary LV fluid inclusions only.

5.1.2. Comparison with *in vacuo* crushing

In vacuo crushing was carried out on samples EL 48177 and AW02-002b and in both cases gave higher Br/Cl values than were obtained by stepped heating (Table 3). In the case of sample EL 48177, which is dominated by high salinity LVD fluid inclusions (Table 1), the difference can be explained by the retention of $^{38}\text{Ar}_\text{Cl}$ in daughter minerals which leads to artificially elevated Br/Cl and I/Cl values during *in vacuo* crushing (Kendrick et al., 2001a).

In contrast, the true Br/Cl and I/Cl values are obtained during stepped heating of the uncrushed sample splits. Daughter mineral retention of $^{38}\text{Ar}_\text{Cl}$ does not appear to be significant during stepped heating because: (1) The vast majority of fluid inclusions homogenise before decrepitation. (2) MS fluid inclusions that decrepitate before complete homogenisation retain only the least soluble daughter minerals such as carbonate or pyrosomalite that are not major reservoirs for Cl or $^{38}\text{Ar}_\text{Cl}$. (3) After decrepitation, and at temperatures of a few hundred degrees, $^{38}\text{Ar}_\text{Cl}$ is readily released from undissolved daughter minerals: stepped heating of halite bearing crushed residues yields very low Br/Cl and I/Cl values at 200 °C, indicating that $^{38}\text{Ar}_\text{Cl}$ is readily liberated from the daughter minerals at this temperature. Therefore, retention of $^{38}\text{Ar}_\text{Cl}$ in undissolved daughter minerals cannot explain the shift to low Br/Cl and I/Cl values that is seen in all samples at 1200–1450 °C.

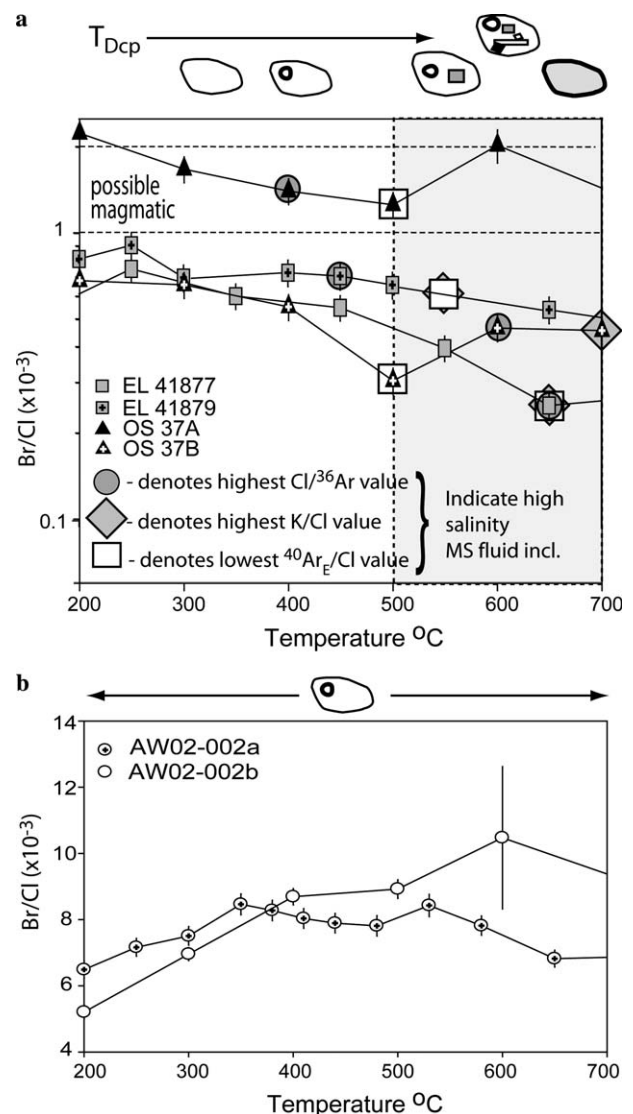


Fig. 13. Br/Cl decrepitation profiles. (a) For the IOCG deposits Eloise and Osborne. The microthermometric observations are summarized above the plot, these and the fluid Ar/Cl and K/Cl values (Fig. 12) indicate that the most saline primary fluid inclusions decrepitated above 500 °C are characterised by the lowest Br/Cl values. (b) The Railway Fault sample contains only LV fluid inclusions. Br/Cl variation in this sample is less systematic. Nb-analytical uncertainty only is shown for these samples.

Daughter minerals were not observed in the wafer of sample AW02-002. Although it is possible that daughter minerals were present in the split analysed, but not in the wafer, two explanations more likely to explain the high Br/Cl values determined by *in vacuo* crushing (Table 3) are: (1) *in vacuo* crushing sampled a different population of fluid inclusions compared to stepped heating, or (2) the splits analysed were from significantly different zones within the sample that had real differences in Br/Cl.

In all the other Mt Isa samples that do not contain fluid inclusions with daughter minerals, *in vacuo* crushing and stepped heating yield similar results (Kendrick, unpublished data). However, the Br/Cl and I/Cl values determined by stepped heating uncrushed samples usually

exhibit greater variation than those determined by in vacuo crushing. This is compatible with the selective decrepitation of different fluid inclusion types at different temperatures during stepped heating and the homogenisation of many different fluid inclusion types during in vacuo crushing.

5.2. Fluid origins

5.2.1. Halogens

The weighted mean Br/Cl and I/Cl values of gas released from each sample, in the temperature range 200–700 °C, have been plotted (large symbols in Fig. 14). The intra-sample variation is indicated by the composition of individual extraction steps (small symbols in Fig. 14) and is far greater than the analytical uncertainty of 1.5–3% for Br/Cl and 3–5% for I/Cl (1σ).

The majority of IOCG samples plot in a field with Br/Cl between 0.3×10^{-3} and 10^{-3} and I/Cl between 10^{-6} and 5×10^{-6} (Fig. 14). These values are lower than the range of values previously determined for Porphyry Copper Deposits (PCD) and Mantle Diamond ($0.9\text{--}2 \times 10^{-3}$ and $8\text{--}100 \times 10^{-6}$, Johnson et al., 2000; Kendrick et al., 2001b), that are considered representative of juvenile magmatic fluids derived from a mantle source. Sample OS 37A lies within the above range, compatible with some involvement of juvenile magmatic fluids in IOCG genesis. Such fluids could be derived from the abundant A-type granites within the Cloncurry district (Baker, 1998; Williams, 1998; Mark et al., 2004).

The lowest Br/Cl and I/Cl values are slightly above those of halite dissolution waters (Fig. 14). These values

may represent either incomplete halite dissolution, where NaBr and NaI have been dissolved preferentially relative to NaCl; or dissolution of other evaporite minerals such as sylvite that accommodate more Br than halite; or it may represent mixing between halite dissolution water and a magmatic fluid. (Barton and Johnson, 1996). In either case, halite dissolution must have occurred at high pressure and temperature to enable the exceptional salinities of ~65 wt%, that are much greater than the salinity of surface brines saturated with halite (26–30 wt%). It is notable that the samples including the highest salinity fluid inclusions, OS 37B and EL 48177, have the least magmatic compositions (Table 1 and Fig. 14), which supports the idea that evaporites may be the most important source of salinity for IOCG genesis (Barton and Johnson, 1996).

An alternative to halite dissolution might be acquisition of Cl by melting of the abundant metamorphic scapolite that is present within the district and formed by metamorphism of evaporitic rocks (Williams, 1998; Mark and Pol-lard, 2003). The distribution coefficient of Br and Cl in scapolite is unity (Pan and Dong, 2003), suggesting that metamorphic scapolite derived from Br-poor evaporitic rocks would also have a Br-poor composition.

AW02-002 has a Br/Cl and I/Cl composition that lies very close to the modern day seawater evaporation trajectory (Fig. 14; Zhrebtsova and Volkova, 1966). Silicic alteration at the Mt Isa mine is characterised by fluid inclusions with similarly elevated Br/Cl values (Heinrich et al., 1993). Such values may represent a bittern brine that has been enriched in iodine subsequent to a sub-aerial origin by the evaporation of seawater beyond the point of halite saturation. Iodine enrichment can take place in the sub-surface as a result of fluid interaction with organic-rich sedimentary rocks (Worden, 1996; Kendrick et al., 2005). As the fluid inclusions are no longer saturated with halite significant dilution must also have taken place.

5.2.2. Argon

The Eloise and Osborne IOCG samples have low $^{40}\text{Ar}/^{36}\text{Ar}$ values from near the atmospheric value of 296, up to a maximum of 2236 in sample OS 37A (Fig. 11) which has the most mantle-like halogen signature (Fig. 14; Table 4). These values are orders of magnitude lower than the MORB mantle $^{40}\text{Ar}/^{36}\text{Ar}$ value of 40,000–44,000 (Burnard et al., 1997; Moreira et al., 1998) and, like the halogens, provide strong evidence that an external meteoric or halite dissolution water component has been involved in mineralisation.

The $^{40}\text{Ar}_\text{E}/\text{Cl}$ values are highly variable lying between 10^{-5} and 10^{-6} (Fig. 11). These values are much lower than the values measured in mantle diamond and the most magmatic PCD fluids (Johnson et al., 2000; Kendrick et al., 2001b) and also favour the involvement of crustal fluids. The maximum $\text{Cl}/^{36}\text{Ar}$ values, the minimum $^{40}\text{Ar}_\text{E}/\text{Cl}$ values and the maximum salinity of primary fluid inclusions indicate that the IOCG fluids have $^{40}\text{Ar}_\text{E}$ concentration of 0.4–3 ppm and ^{36}Ar concentration of 1–6 ppb (Table 4).

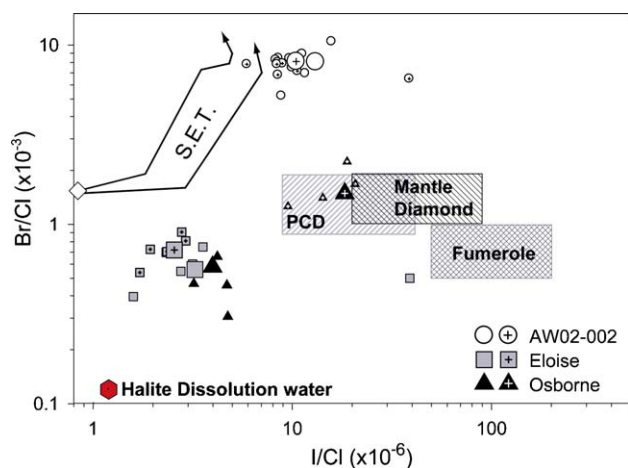


Fig. 14. Br/Cl and I/Cl data for quartz samples from Eloise, Osborne and the Railway Fault. Large data points represent the weighted mean of gas released in the temperature interval 200–700 °C, small data points represent the composition of individual extraction steps. The empty and crossed symbols distinguish individual samples for each of the localities and are the same as in all other figures. The compositions of halite dissolution water (Böhlke and Irwin, 1992b), seawater, the seawater evaporation trajectory (S.E.T.; Zhrebtsova and Volkova, 1966) and the composition of possible magmatic fluids derived from the mantle (Porphyry Copper Deposit fluids PCD, mantle diamond and volcanic fumeroles; Kendrick et al., 2001b and references therein) are shown for reference.

Table 4
Summary of compositions determined for primary fluid inclusions^a

Sample	⁴⁰ Ar/ ³⁶ Ar	Cl/ ³⁶ Ar × 10 ⁶	⁴⁰ Ar _E /Cl × 10 ^{−6}	Salinity wt. %	Max. [³⁶ Ar]		Max. [⁴⁰ Ar _E]		Br/Cl (× 10 ^{−3})	I/Cl (× 10 ^{−6})	K/Cl ^b
					cm ³ cm ^{−3} H ₂ O × 10 ^{−6}	ppb	cm ³ cm ^{−3} H ₂ O × 10 ^{−3}	ppm			
<i>Eloise</i>											
EL 48177	708–1082	257	3.1	50	0.7	1	0.6	1	0.25–0.40	0.37–1.7	0.09–0.13
EL 48179	360–800	146	3.8–8.9	40	1.0	2	0.6–1.4	1–3	0.54–0.66	0.39–1.8	0.16–0.20
<i>Osborne</i>											
OS 37A	380–2236	49	4.4	45	3.5	6	0.8	1	1.3–2.0	10	
OS 37B	460–570	289	0.7–1.0	65	0.9	1	0.2–0.3	0.4–0.5	0.31–0.47	3.4–5.0	0.14–0.27
<i>Railway Fault</i>											
AW02-002a	1921 ^c	9.8		12	4.7	8			8.1	9.4	
AW02-002b	730 ^c	5.9		12	7.8	13			8.1	12	(<0.7–0.8 ^e)
<i>Reference values</i> ^d											
Meteoritic	295			0	1–1.7	1.6–2.7	0	0	—	—	
Halite dissolution		≫0		High					0.1	1.2	
Seawater	295	10–17	0	3.5	0.8–1.3	1.3–2.1	0	0	1.54	0.86	
MORB mantle	>40 000	10–30	1000	<8 to ?	<0.1	<0.16	1–3	1.8–5.4	0.9–2	9.3–40	

^a The ranges of ⁴⁰Ar/³⁶Ar, Br/Cl, I/Cl and K/Cl values given for the IOCG samples (Eloise and Osborne) were determined in the temperature interval 500 to 700 °C, that is dominated by the decrepitation of primary MS and LVD fluid inclusions. Sample AW02–002 from the Railway Fault includes only primary LV fluid inclusions and so the ranges of Br/Cl, I/Cl and K/Cl values were determined over the temperature interval 200–700 °C. The salinities represent the mean values of the highest-salinity fluid inclusion-type present (MS, LVD, or LV). In order to minimise the effects of atmospheric contamination, the ³⁶Ar concentration is calculated using the sample maximum Cl/³⁶Ar value. The ⁴⁰Ar_E/Cl values represent the minimum determined in the temperature range 400 to 700 °C that should be most characteristic of high salinity fluid inclusions. Where there was significant variation in the ⁴⁰Ar_E/Cl value, within this range, the sample mean value is included as an upper limit.

^b Fluid inclusion K/Cl values obtained by stepped heating can be compromised if very minor K-mineral impurities are present. The K/Cl value determined at 600 °C for sample OS 37A is slightly >1 indicating such a mineral impurity, representative values are included for OS 37B.

^c The ⁴⁰Ar/³⁶Ar values determined for sample AW02-002 are averaged over the entire experiment. The implications of the accidentally trapped mica in this sample for determination of the initial ⁴⁰Ar/³⁶Ar values are discussed fully in Part II (Kendrick et al., 2006).

^d Reference values in Böhlke and Irwin (1992b), Burnard et al. (1997), Moreira et al. (1998), Johnson et al. (2000), Kendrick et al. (2001b), and Ozima and Podsek (2002).

^e Sample AW02-002 includes very significant accidentally trapped mica (max K/Cl > 500). The K/Cl value determined by in vacuo crushing, which selectively samples the fluid inclusions, remains unrealistically high at 0.7–0.8 and suggests that some recoil-loss of ³⁹Ar_K has occurred from the mica into the fluid inclusions (Kendrick et al., 2006).

The concentration of ^{36}Ar is slightly lower than that of meteoric water, in the majority of samples that have halite dissolution-like halogen signatures, but sample OS 37A with the magmatic-like halogen signature is enriched in ^{36}Ar relative to either meteoric water or mantle fluids (Table 4).

The correction for post-entrapment in situ production of radiogenic $^{40}\text{Ar}_\text{R}$ is straight forward for the IOCG samples, but in sample AW02-002 it is complicated by the presence of accidentally trapped mica in the fluid inclusions. The analytical implications of the accidentally trapped mica are evaluated fully in Part II (Kendrick et al., 2005); here we note only that the sample has a mean $^{40}\text{Ar}/^{36}\text{Ar}$ value of <2000 (Table 4). This is slightly higher than the maximum values determined for the composition of ore fluids in several MVT districts (Kendrick et al., 2002a,b). The maximum $\text{Cl}/^{36}\text{Ar}$ value of $5.9\text{--}9.8 \times 10^6$ and the mean salinity of ~ 12 wt% NaCl eq. indicate a ^{36}Ar concentration of 8–13 ppb, significantly above the concentration in meteoric water (Table 4). The noble gas and halogen data are compatible with the origin of this fluid as a basinal brine that has been enriched in atmospheric noble gases through interaction with fine grained sedimentary rocks.

Measurement of the heavier, atmospheric noble gases ^{84}Kr and ^{129}Xe was compromised at temperatures of <600 °C by a blank component associated with the Cu-foil packaging (Section 3.3). The F^{84}Kr and F^{129}Xe values obtained by in vacuo crushing and at temperatures of over 600 °C encompass a range from significantly less than the air value of one up to values of greater than ASW (Appendix B). The range in values cannot be explained by mixing between air and ASW alone; phase separation or interaction with fine grained organic-rich sediments may explain the additional fractionation. However, due to the lack of data at <600 °C, that can be correlated with decrepitation of a given population of fluid inclusions, we make no further comment.

6. Conclusions

Fluid inclusions are the dominant reservoir for noble gases and halogens in quartz. During stepped heating they degas bimodally in two decrepitation related degassing peaks. Compositional variation in Br/Cl and I/Cl within the first degassing peak (<700 °C) can be related to the different decrepitation temperatures of different types of fluid inclusion determined by microthermometry. Variations in Cl/Ar and K/Cl can be used as imperfect proxies to confirm if the K-rich ultra-high-salinity fluid inclusions are decrepitated in the expected ranges.

In all the samples analysed, a greater volume of gas is released from fluid inclusions between 1200 and 1450 °C during the second degassing peak, than is released from fluid inclusions at <700 °C. The Br/Cl and I/Cl composition of this gas is systematically shifted to lower values than

are obtained at <700 °C. Release of this gas is probably triggered by a phase transition of quartz and the gas is released from the smallest fluid inclusions within the sample. The low Br/Cl and I/Cl values may indicate that either the small fluid inclusions have non-representative compositions or that diffusion fractionates the noble gas elemental compositions at high temperature. Ar-isotopes are unaffected and appear representative of fluid inclusion compositions at all temperatures. Fluid inclusions undecrepitated at 1200 °C need to be accounted for in models explaining H-isotope fractionation between matrix and fluid inclusion reservoir sites.

The study has demonstrated the potential of the noble gas and halogen technique to investigate Proterozoic ore deposits with complex fluid inclusion assemblages. Ultra-high salinity, primary fluid inclusions, in three IOCG samples from Eloise and Osborne have Br/Cl and I/Cl values of $0.25\text{--}0.66 \times 10^{-3}$ and $0.37\text{--}5.0 \times 10^{-6}$. One of the Osborne samples includes fluids with higher values that are similar to Porphyry Copper Deposits, compatible with the involvement of a juvenile magmatic fluid (e.g., Baker, 1998; Williams, 1998). However, it is the highest salinity samples that have compositions least similar to the magmatic range, suggesting that interaction with evaporites is important. Like the halogens, the $^{40}\text{Ar}/^{36}\text{Ar}$ of <2000 and $^{40}\text{Ar}_\text{E}/\text{Cl}$ values of $10^{-5}\text{--}10^{-6}$ measured in IOCG fluids are most easily explained by the involvement of external crustal fluids.

The Railway Fault sample has basic thermometric properties that are similar to silicic alteration at the Mt Isa mine. The Br/Cl values are also similar at $\sim 8.1 \times 10^{-3}$, and together with I/Cl of $9.4\text{--}12 \times 10^{-6}$, $^{40}\text{Ar}/^{36}\text{Ar}$ of <2000 and ^{36}Ar concentration of 8–13 ppb, are compatible with an origin by the evaporation of seawater beyond the point of halite saturation and subsequent interaction with I-rich sedimentary rocks in the subsurface plus dilution to 12 wt% NaCl eq.

The intra- and inter-sample variation for each of the deposits studied is large and more detailed work is required to better understand the genesis of the diverse mineralization types within the Mt Isa Inlier.

Acknowledgments

This work was funded under the Predictive Mineral Discovery Cooperative Research Centre (pmd*CR) fluid history project (H4), and is published with permission. We thank Stan Szczepanski for technical assistance in the laboratory. The samples EL 48177, EL48179, OS37A, OS37B and AW02-002 were kindly provided by Tim Baker, Roger Mustard and Andy Wilde. M.K. has benefited from discussions with Louise Fisher. We thank Andy Hunt and an anonymous GCA reviewer, as well as the associate editor Bob Burruss, for constructive comments that improved the manuscript.

Associate editor: Robert C. Burruss

Appendix A. Irradiation UM#4 undertaken on the 30-Nov-2003

$$J = 0.0186 \pm 0.0001 \quad \beta = 4.8 \pm 0.3 \quad \alpha = 0.55 \pm 0.01$$

J , β and α are determined experimentally from the Hb3Gr standard using the known age and K/Cl plus K/Ca weight ratios (Kelley et al., 1986).

$$J = (e^{Jt} - 1) / ({}^{40}\text{Ar}_R / {}^{39}\text{Ar}_K)$$

$$\beta = (\text{K}/\text{Cl}) / ({}^{39}\text{Ar}_K / {}^{38}\text{Ar}_{\text{Cl}})$$

$$\alpha = (\text{K}/\text{Ca}) / ({}^{39}\text{Ar}_K / {}^{37}\text{Ar}_{\text{Ca}})$$

Calculated neutron flux

$$\text{Thermal flux}(\phi_t) = 9.6 \times 10^{18} \pm 0.6 \times 10^{18}$$

$$\text{Fast flux}(\phi_f) = 3.52 \times 10^{18} \pm 0.02 \times 10^{18}$$

Standard Ar interference corrections obtained from salts

$${}^{36}\text{Ar}/{}^{37}\text{Ar}_{\text{Ca-salt}} = 0.000322 \pm 0.000012$$

$${}^{39}\text{Ar}/{}^{37}\text{Ar}_{\text{Ca-salt}} = 0.000685 \pm 0.000009$$

$${}^{38}\text{Ar}/{}^{39}\text{Ar}_{\text{K-salt}} = 0.0124 \pm 0.0001$$

$${}^{40}\text{Ar}/{}^{39}\text{Ar}_{\text{K-salt}} = 0.0295 \pm 0.0023$$

Table A.1

Calculation of parent elements

Reaction	Important neutrons	Calculation	Equation
${}^{39}\text{K}(\text{n},\text{p}){}^{39}\text{Ar}$	Fast	$\text{K mols} = {}^{39}\text{Ar}_K \text{ cm}^3 \text{ STP} \times (3.647/J)$	(1)
${}^{40}\text{Ca}(\text{n},\alpha){}^{37}\text{Ar}$	Fast	$\text{Ca mols} = {}^{37}\text{Ar}_{\text{Ca}} \text{ cm}^3 \text{ STP} \times (3.558/J\alpha)$	(2)
${}^{37}\text{Cl}(\text{n},\gamma\beta){}^{38}\text{Ar}$	Thermal	$\text{Cl mols} = {}^{38}\text{Ar}_{\text{Cl}} \text{ cm}^3 \text{ STP} \times (4.022/\beta J)$ or $\text{Cl mols} = \frac{{}^{38}\text{Ar}_{\text{Cl}} \text{ mols}}{\phi_t \times \sigma_t \times {}^{37}\text{Cl}/\text{Cl} \times Y}$	(3) (4)
${}^{79}\text{Br}(\text{n},\gamma\beta){}^{80}\text{Kr}$	Thermal + resonant*	$\text{Br mols} = \frac{{}^{80}\text{Kr}_{\text{Br}} \text{ mols}}{\phi_t \times \sigma_t \times {}^{79}\text{Br}/\text{Br} \times Y} \div R^*$	(5)
${}^{127}\text{I}(\text{n},\gamma\beta){}^{128}\text{Xe}$	Thermal + resonant*	$\text{I mols} = \frac{{}^{128}\text{Xe}_{\text{I}} \text{ mols}}{\phi_t \times \sigma_t \times Y} \div R^*$	(6)

Where; ϕ_t , thermal neutron flux; σ_t , thermal neutron reaction cross section; Y , yield (values given in Irwin and Reynolds, 1995). R^* , resonance correction factors of 1.3 for Br and 1.7 for I, based on several previous irradiations (Johnson et al., 2000; Kendrick et al., 2001a; 2002a; 2005a; unpublished data). $\text{Nb}-{}^{37}\text{Ar}_{\text{Ca}}$ is corrected for post-irradiation radioactive decay.

The calculation of Br and I based on thermal neutrons only is a simplification that necessitates incorporation of a resonant neutron correction factor. Dividing Eqs. (5) and (6) by Eq. (4) gives:

$$\frac{\text{Br}}{\text{Cl}} = \frac{{}^{80}\text{Kr}_{\text{Br}}}{{}^{38}\text{Ar}_{\text{Cl}}} \times \text{constant} \div R^* \quad \frac{\text{I}}{\text{Cl}} = \frac{{}^{128}\text{Xe}_{\text{I}}}{{}^{38}\text{Ar}_{\text{Cl}}} \times \text{constant} \div R^*.$$

The constants above incorporate the isotopic ratios, yields and thermal neutron cross sections of Eqs. (4)–(6). The flux of thermal neutrons cancels out when Eq. (5) or (6) is divided by Eq. (4). The only variables are therefore the measured isotopic ratio and the resonant neutron correction factor. The total uncertainty of 10% (1σ) for both Br/Cl and I/Cl is based on the variability of the resonance neutron correction factor in previous irradiations and in this instance only, is greater than the analytical uncertainty of 1.5–3% for Br/Cl and 3–5% for I/Cl. The calculations are summarized in Table A.1.

Appendix B. Noble gas and halogen data

The tabulated data is corrected for Ar-interference reactions and post-irradiation isotope decay. The ${}^{40}\text{Ar}_{\text{corr}}$ value is the measured ${}^{40}\text{Ar}$ value corrected for post-entrapment radiogenic production of ${}^{40}\text{Ar}_R$, based upon the measured K abundance of each step and the ages for Eloise of 1530 Ma (Baker et al., 2001), for Osborne of 1595 Ma (Gauthier et al., 2001) and an assumed age of 1523 Ma for the Railway Fault (see Part II, Kendrick et al., 2006). The uncorrected values are given in the appendix of Part II. The molar Br/Cl and I/Cl ratios are given in preference to Br and I abundances, because they have lower uncertainty.

Temperature (°C)	$^{40}\text{Ar}_{\text{corr}}$ mols ($\times 10^{-15}$)	^{36}Ar mols ($\times 10^{-15}$)	^{84}Kr mols ($\times 10^{-18}$)	^{129}Xe mols ($\times 10^{-18}$)	Cl mols ($\times 10^{-9}$)	K mols ($\times 10^{-9}$)	Br/Cl ($\times 10^{-3}$)	I/Cl ($\times 10^{-6}$)
Eloise								
<i>EL 48177 combined crushing and stepped heating data (22.5 mg)</i>								
Cr 1	28.0 \pm 0.1	0.17 \pm 0.01	0.19 \pm 0.01	0.28 \pm 0.09	1.29 \pm 0.08			
Cr 2	2336.7 \pm 7.6	2.46 \pm 0.01	56.6 \pm 1.5	0.22 \pm 0.09	142 \pm 9	6.19 \pm 0.04	0.89 \pm 0.09	1.5 \pm 0.2
Cr 3	1029.2 \pm 2.3	0.73 \pm 0.01	18.1 \pm 0.5		78.9 \pm 5.1	3.34 \pm 0.02	0.87 \pm 0.09	5.5 \pm 0.6
200	140.31 \pm 0.0	0.35 \pm 0.01			18.0 \pm 1.2		0.11 \pm 0.01	0.35 \pm 0.04
300	235.9 \pm 0.5	0.31 \pm 0.01			14.0 \pm 0.9	0.41 \pm 0.01	0.27 \pm 0.03	1.2 \pm 0.1
400	226.7 \pm 0.7	0.39 \pm 0.01			35.4 \pm 2.3	1.14 \pm 0.03	0.25 \pm 0.03	1.0 \pm 0.1
500	110.1 \pm 0.5	0.135 \pm 0.003			23.1 \pm 1.5	1.88 \pm 0.02	0.32 \pm 0.03	0.8 \pm 0.1
600	20.2 \pm 0.4	0.224 \pm 0.002			3.9 \pm 0.3	1.75 \pm 0.02	0.45 \pm 0.05	
800	28.9 \pm 0.7	0.02 \pm 0.01	0.74 \pm 0.01		7.0 \pm 0.5	2.1 \pm 0.2	0.44 \pm 0.04	2.7 \pm 0.3
1000	46.4 \pm 0.6	0.04 \pm 0.01	0.43 \pm 0.22		5.5 \pm 0.4	1.9 \pm 0.2	0.54 \pm 0.05	1.6 \pm 0.2
1200	299.4 \pm 1.6	0.42 \pm 0.01	5.98 \pm 0.10		25.5 \pm 1.7	1.6 \pm 0.1	0.44 \pm 0.05	2.7 \pm 0.3
1400	792.6 \pm 2.7	0.51 \pm 0.01	7.56 \pm 0.16	0.43 \pm 0.02	60.9 \pm 4.0	2.9 \pm 0.1	0.45 \pm 0.05	2.6 \pm 0.3
Total	5294 \pm 9	5.76 \pm 0.04			416 \pm 12	23.2 \pm 0.3		
<i>EL 48177 stepped heating data (26.0 mg)</i>								
150	25.8 \pm 0.2	0.14 \pm 0.01			0.06 \pm 0.01	0.17 \pm 0.02		
250	675.9 \pm 1.8	0.79 \pm 0.01			16.8 \pm 1.1	1.04 \pm 0.08	0.75 \pm 0.08	3.7 \pm 0.4
350	866.8 \pm 2.3	0.71 \pm 0.03			54.2 \pm 3.5	1.60 \pm 0.04	0.60 \pm 0.06	3.3 \pm 0.4
450	919.7 \pm 2.5	0.72 \pm 0.01			118 \pm 8	4.15 \pm 0.03	0.55 \pm 0.06	2.9 \pm 0.3
550	99.5 \pm 0.4	0.141 \pm 0.003			17.2 \pm 1.1	1.60 \pm 0.05	0.40 \pm 0.04	1.7 \pm 0.2
650	22.2 \pm 0.2	0.02 \pm 0.02	0.68 \pm 0.02		5.3 \pm 0.3	0.70 \pm 0.03	0.25 \pm 0.03	0.4 \pm 0.1
800	22.2 \pm 0.4	0.14 \pm 0.01	1.93 \pm 0.03		7.0 \pm 0.5	1.52 \pm 0.07	0.28 \pm 0.03	1.2 \pm 0.1
1000	58.3 \pm 1.0	0.13 \pm 0.05	1.31 \pm 0.07		6.0 \pm 0.4	1.33 \pm 0.07	0.56 \pm 0.06	1.3 \pm 0.2
1200	1497.7 \pm 4.3	0.76 \pm 0.01	20.7 \pm 1.1	0.91 \pm 0.08	178 \pm 12	8.34 \pm 0.07	0.48 \pm 0.05	2.9 \pm 0.3
Total	4188 \pm 6	3.56 \pm 0.06			402 \pm 14	20.4 \pm 0.2		
<i>EL 48179 stepped heating data (92.0 mg)</i>								
200	326.7 \pm 0.5	0.30 \pm 0.02			2.1 \pm 0.1	0.32 \pm 0.09	0.81 \pm 0.09	3.06 \pm 1.3
250	1245.6 \pm 3.2	0.606 \pm 0.004			12.9 \pm 0.8	0.34 \pm 0.07	0.91 \pm 0.10	2.92 \pm 0.4
300	692.2 \pm 1.5	0.43 \pm 0.01			20.1 \pm 1.3	0.38 \pm 0.00	0.70 \pm 0.07	2.44 \pm 0.3
350	375.6 \pm 0.5	0.32 \pm 0.01			22.0 \pm 1.4	0.93 \pm 0.06	0.71 \pm 0.08	2.35 \pm 0.2
400	399.9 \pm 1.1	0.37 \pm 0.01			24.4 \pm 1.6	0.64 \pm 0.03	0.73 \pm 0.08	2.03 \pm 0.2
450	485.0 \pm 1.4	0.41 \pm 0.02			29.0 \pm 1.9	1.07 \pm 0.06	0.71 \pm 0.08	2.46 \pm 0.3
500	68.9 \pm 0.5	0.10 \pm 0.03			3.6 \pm 0.2	0.58 \pm 0.36	0.66 \pm 0.07	0.39 \pm 0.3
550	35.4 \pm 0.2	0.098 \pm 0.003			1.8 \pm 0.1	0.35 \pm 0.07		
650	51.1 \pm 0.3	0.064 \pm 0.002	1.4 \pm 0.2	0.44 \pm 0.03	2.4 \pm 0.2	0.43 \pm 0.03	0.54 \pm 0.06	1.80 \pm 0.5
800	74.6 \pm 0.3	0.14 \pm 0.01	1.3 \pm 0.2	0.48 \pm 0.02	4.9 \pm 0.3	0.95 \pm 0.05	0.45 \pm 0.05	2.75 \pm 0.3
1000	113.9 \pm 0.4	0.26 \pm 0.01	2.7 \pm 0.1	0.53 \pm 0.05	9.1 \pm 0.6	1.39 \pm 0.01	0.48 \pm 0.05	1.99 \pm 0.2
1100	198.4 \pm 1.2	0.349 \pm 0.004	4.4 \pm 0.2	0.42 \pm 0.02	13.2 \pm 0.9	0.94 \pm 0.01	0.52 \pm 0.06	1.93 \pm 0.2
1200	1341.7 \pm 3.9	0.86 \pm 0.01	22.3 \pm 0.9	1.28 \pm 0.08	113 \pm 7	5.40 \pm 0.05	0.51 \pm 0.05	2.27 \pm 0.2
1300	680.6 \pm 1.7	0.56 \pm 0.01	7.3 \pm 0.4	0.42 \pm 0.14	63.9 \pm 4.1	3.29 \pm 0.02	0.22 \pm 0.02	0.87 \pm 0.1
1400	853.7 \pm 2.4	0.53 \pm 0.01	5.3 \pm 0.2	0.42 \pm 0.06	78.0 \pm 5.1	3.80 \pm 0.05	0.19 \pm 0.02	0.73 \pm 0.1
Total	6943 \pm 6	5.41 \pm 0.05			400 \pm 10	20.8 \pm 0.4		
Osborne								
<i>OS 37A stepped heating data (41.9 mg)</i>								
200	158.9 \pm 0.5	0.52 \pm 0.01			0.81 \pm 0.05	0.19 \pm 0.01	2.2 \pm 0.2	19.8 \pm 2.0
300	186.8 \pm 0.9	0.25 \pm 0.01			5.2 \pm 0.3	0.13 \pm 0.03	1.7 \pm 0.2	21.7 \pm 2.2
400	190.9 \pm 0.3	0.296 \pm 0.004			14.5 \pm 0.9	0.89 \pm 0.02	1.4 \pm 0.1	14.9 \pm 1.5
200	22.9 \pm 0.3	0.060 \pm 0.002			1.15 \pm 0.08	0.76 \pm 0.07	1.3 \pm 0.1	10.0 \pm 1.2
600	25.9 \pm 0.2	0.012 \pm 0.004			0.15 \pm 0.02	0.17 \pm 0.16	2.0 \pm 0.3	

Appendix B (continued)

Temperature (°C)	⁴⁰ Ar _{corr} mols (×10 ⁻¹⁵)	³⁶ Ar mols (×10 ⁻¹⁵)	⁸⁴ Kr mols (×10 ⁻¹⁸)	¹²⁹ Xe mols (×10 ⁻¹⁸)	Cl mols (×10 ⁻⁹)	K mols (×10 ⁻⁹)	Br/Cl (×10 ⁻³)	I/Cl (×10 ⁻⁶)
800	24.8 ± 0.4	0.030 ± 0.004	1.78 ± 0.18	0.68 ± 0.02	0.45 ± 0.03	1.08 ± 0.08	1.0 ± 0.1	8.6 ± 1.6
1000	56.7 ± 2.4	0.13 ± 0.02	3.99 ± 0.17	0.78 ± 0.10	0.38 ± 0.03	1.75 ± 0.05	3.2 ± 0.3	27.8 ± 7.4
1200	113.4 ± 0.7	0.30 ± 0.01	8.28 ± 0.29	1.62 ± 0.03	1.92 ± 0.13	3.23 ± 0.04	1.6 ± 0.2	15.2 ± 1.7
1400	340.9 ± 0.9	0.84 ± 0.01	21.4 ± 0.9	3.63 ± 0.10	10.4 ± 0.7	1.56 ± 0.09	1.1 ± 0.1	8.0 ± 0.8
1600	766.5 ± 2.5	2.12 ± 0.01	79.5 ± 2.3	15.1 ± 0.3	11.7 ± 0.8	3.41 ± 0.06	2.8 ± 0.3	11.6 ± 1.2
Total	1888 ± 4	4.57 ± 0.03			47 ± 1	13.2 ± 0.2		
<i>OS 37B stepped heating data (43.2 mg)</i>								
200	218.5 ± 0.8	0.718 ± 0.005			4.5 ± 0.3		0.68 ± 0.07	
300	185.7 ± 0.3	0.391 ± 0.005			25.8 ± 1.7	2.37 ± 0.01	0.66 ± 0.07	4.4 ± 0.5
400	125.5 ± 1.0	0.312 ± 0.003			33.0 ± 2.1	2.60 ± 0.04	0.55 ± 0.06	3.4 ± 0.4
500	34.0 ± 0.7	0.12 ± 0.01			0.8 ± 0.1	0.22 ± 0.04	0.31 ± 0.03	5.0 ± 0.7
600	52.0 ± 0.7	0.11 ± 0.01			12.9 ± 0.8	1.8 ± 0.1	0.47 ± 0.05	3.4 ± 0.4
700	11.0 ± 0.2	0.02 ± 0.01	1.04 ± 0.08	0.12 ± 0.10	0.8 ± 0.1	0.55 ± 0.03	0.46 ± 0.05	4.9 ± 1.6
800	11.0 ± 0.2		0.28 ± 0.12	0.092 ± 0.002	0.7 ± 0.0	0.67 ± 0.01	0.55 ± 0.06	2.0 ± 1.0
1000	13.3 ± 0.3	0.07 ± 0.01	1.11 ± 0.12	0.52 ± 0.01	1.7 ± 0.1	0.60 ± 0.11	0.61 ± 0.06	5.3 ± 0.8
1200	210.8 ± 1.0	0.29 ± 0.01	7.88 ± 0.21	0.73 ± 0.03	84.8 ± 5.5	9.9 ± 0.1	0.48 ± 0.05	3.8 ± 0.4
1400	146.5 ± 0.9	0.326 ± 0.004	8.59 ± 0.25	1.24 ± 0.02	40.0 ± 2.6	5.62 ± 0.03	0.22 ± 0.02	1.0 ± 0.1
1600	212.1 ± 1.4	0.62 ± 0.04	19.8 ± 0.7			38.5 ± 2.5	5.7 ± 0.1	0.49 ± 0.05
Total	1221 ± 3	2.99 ± 0.05			243.6 ± 7.2	30.0 ± 0.2		
<i>Railway Fault</i>								
<i>AW02-002a stepped heating data (126 mg)</i>								
150	27.7 ± 0.1	0.10 ± 0.003						
200	446.8 ± 1.4	0.91 ± 0.01			0.64 ± 0.04	0.90 ± 0.04	6.5 ± 0.7	40.5 ± 4.9
250	1363.7 ± 4.3	2.01 ± 0.02			3.0 ± 0.2	5.94 ± 0.05	7.2 ± 0.8	11.1 ± 1.2
300	2799.3 ± 9.3	2.23 ± 0.02			9.6 ± 0.6	15.6 ± 0.1	7.5 ± 0.8	10.4 ± 1.1
350	6944.3 ± 23.0	3.91 ± 0.03			29.9 ± 1.9	37.9 ± 0.3	8.5 ± 0.9	8.9 ± 0.9
380	3471.6 ± 11.4	1.56 ± 0.01			15.3 ± 1.0	40.7 ± 0.2	8.3 ± 0.9	8.7 ± 0.9
410	2869.7 ± 12.2	1.46 ± 0.01			11.4 ± 0.7	78.7 ± 0.5	8.0 ± 0.9	8.8 ± 0.9
440	2658.7 ± 14.8	1.63 ± 0.02			9.9 ± 0.6	116.0 ± 0.7	7.9 ± 0.8	9.3 ± 1.0
480	566.8 ± 14.8	0.51 ± 0.01			2.1 ± 0.1	161.6 ± 1.0	7.8 ± 0.8	8.8 ± 0.9
530	270.2 ± 17.0	0.31 ± 0.01			1.1 ± 0.1	187.7 ± 1.2	8.4 ± 0.9	10.1 ± 1.1
580	149.5 ± 15.4	0.23 ± 0.00			0.66 ± 0.04	174.0 ± 1.1	7.8 ± 0.8	6.2 ± 3.2
650	80.5 ± 15.0	0.28 ± 0.02	4.4 ± 0.5	0.20 ± 0.02	0.68 ± 0.04	168.7 ± 1.0	6.8 ± 0.7	8.9 ± 4.6
750	873.7 ± 16.4	0.56 ± 0.03	13.2 ± 0.6	0.62 ± 0.05	2.7 ± 0.2	174.0 ± 1.0	6.9 ± 0.7	11.0 ± 1.3
850	271.3 ± 8.7	0.28 ± 0.06	7.5 ± 0.3	0.26 ± 0.01	1.2 ± 0.1	103.0 ± 0.6	5.3 ± 0.6	9.2 ± 1.1
1000	1402.0 ± 14.6	0.88 ± 0.02	13.0 ± 0.5	1.02 ± 0.02	5.5 ± 0.4	143.7 ± 0.9	5.8 ± 0.6	7.5 ± 0.9
1100	2069.0 ± 16.0	1.17 ± 0.04	17.3 ± 0.6	1.94 ± 0.06	8.0 ± 0.5	137.2 ± 0.9	5.0 ± 0.5	5.0 ± 0.5
1200	9100.1 ± 36.6	5.15 ± 0.04	56.7 ± 2.1	2.48 ± 0.10	28.6 ± 1.9	198.7 ± 1.2	4.3 ± 0.5	4.3 ± 0.5
1250	12064.1 ± 41.1	5.47 ± 0.04	55.0 ± 2.0	2.45 ± 0.07	39.1 ± 2.5	206.1 ± 1.2	3.7 ± 0.4	3.8 ± 0.4
1290	10717.0 ± 37.3	4.70 ± 0.04	48.8 ± 2.3	2.75 ± 0.06	34.0 ± 2.2	197.9 ± 1.2	3.1 ± 0.3	2.6 ± 0.3
1330	9208.4 ± 31.0	4.20 ± 0.03	42.1 ± 1.9	1.74 ± 0.12	27.0 ± 1.8	158.4 ± 1.0	2.8 ± 0.3	2.7 ± 0.3
1370	8358.4 ± 27.4	4.06 ± 0.04	44.3 ± 1.6	1.23 ± 0.26	22.7 ± 1.5	116.6 ± 0.7	3.1 ± 0.3	3.4 ± 0.4
1410	8187.9 ± 24.9	3.70 ± 0.03	44.5 ± 1.6	1.85 ± 0.15	20.1 ± 1.3	88.8 ± 0.5	3.7 ± 0.4	4.4 ± 0.5
1450	8245.0 ± 24.4	3.51 ± 0.02	71.2 ± 2.6	2.56 ± 0.14	17.5 ± 1.1	72.0 ± 0.4	6.6 ± 0.7	9.3 ± 1.0
1490	5628.5 ± 15.1	2.16 ± 0.01	117 ± 4	4.57 ± 0.20	10.9 ± 0.7	40.6 ± 0.3	18 ± 2	27 ± 3
1530	1827.9 ± 2.8	0.77 ± 0.01	114 ± 4	5.78 ± 0.19	3.6 ± 0.2	12.28 ± 0.08	63 ± 7	115 ± 12
1550	308.7 ± 0.9	0.27 ± 0.02	66.6 ± 2.1	4.44 ± 0.12	0.73 ± 0.05	2.29 ± 0.02	200 ± 21	499 ± 52
Total	99911 ± 103	52.0 ± 0.1			306 ± 5	2639 ± 4		
<i>AW02-002b combined crushing and stepped heating data (22.9 mg)</i>								
Cr 1	128.6 ± 0.6	0.24 ± 0.03	2.9 ± 0.1	0.52 ± 0.03	0.53 ± 0.04	0.35 ± 0.03	9.2 ± 1.0	10.1 ± 1.4

(continued on next page)

Appendix B (continued)

Temperature (°C)	$^{40}\text{Ar}_{\text{corr}}$ mols ($\times 10^{-15}$)	^{36}Ar mols ($\times 10^{-15}$)	^{84}Kr mols ($\times 10^{-18}$)	^{129}Xe mols ($\times 10^{-18}$)	Cl mols ($\times 10^{-9}$)	K mols ($\times 10^{-9}$)	Br/Cl ($\times 10^{-3}$)	I/Cl ($\times 10^{-6}$)
Cr 2	273.0 \pm 0.7	0.51 \pm 0.02	9.7 \pm 0.3	0.44 \pm 0.01	1.34 \pm 0.10	0.94 \pm 0.05	10.9 \pm 1.2	13.4 \pm 1.7
Cr 3	1126.8 \pm 2.4	1.89 \pm 0.01	35.2 \pm 1.2	1.8 \pm 0.1	4.3 \pm 0.3	3.44 \pm 0.05	12.6 \pm 1.3	12.9 \pm 1.3
Cr 4	2634.6 \pm 7.2	2.93 \pm 0.02	66.5 \pm 1.8	2.9 \pm 0.1	10.7 \pm 0.7	7.69 \pm 0.05	11.9 \pm 1.2	16.2 \pm 1.7
Cr 5	2675.6 \pm 6.0	3.11 \pm 0.02	68.2 \pm 1.9	3.6 \pm 0.1	10.3 \pm 0.7	8.52 \pm 0.05	12.6 \pm 1.3	18.8 \pm 1.9
Cr 6	1669.5 \pm 3.0	1.81 \pm 0.02	45.5 \pm 1.2	2.5 \pm 0.2	8.0 \pm 0.5	6.46 \pm 0.06	12.4 \pm 1.3	15.9 \pm 1.7
200	330.9 \pm 1.1	1.01 \pm 0.01			0.26 \pm 0.03	2.69 \pm 0.04	5.7 \pm 0.8	18.9 \pm 2.9
300	300.0 \pm 0.9	0.65 \pm 0.01			0.86 \pm 0.06	8.91 \pm 0.06	5.9 \pm 0.6	12.9 \pm 1.5
400	373.8 \pm 3.3	0.64 \pm 0.02			2.6 \pm 0.2	34.9 \pm 0.2	5.4 \pm 0.6	8.5 \pm 1.1
500	180.5 \pm 12.2	0.27 \pm 0.01			0.71 \pm 0.07	130.7 \pm 1.0	8.4 \pm 1.1	14.1 \pm 1.8
600		0.189 \pm 0.002			0.14 \pm 0.01	74.5 \pm 0.5	9.5 \pm 1.0	27.6 \pm 7.6
800		0.13 \pm 0.03	2.1 \pm 0.1	0.7 \pm 0.0	0.36 \pm 0.04	43.4 \pm 0.3	6.7 \pm 0.9	4.8 \pm 1.2
1000	32.3 \pm 1.6	0.196 \pm 0.004	3.2 \pm 0.1	0.7 \pm 0.1	0.27 \pm 0.02	15.7 \pm 0.1	6.4 \pm 0.7	19.7 \pm 7.4
1200	333.6 \pm 2.7	0.67 \pm 0.01	12.7 \pm 0.4	3.6 \pm 0.1	1.32 \pm 0.09	23.8 \pm 0.1	4.4 \pm 0.5	12.5 \pm 1.4
1400	2383.0 \pm 10.9	3.57 \pm 0.02	53.6 \pm 1.4	6.1 \pm 0.2	11.9 \pm 0.8	45.4 \pm 0.3	5.9 \pm 0.6	3.8 \pm 0.4
1600	2730.7 \pm 7.9	5.78 \pm 0.09	198 \pm 6	29.5 \pm 0.8	7.2 \pm 0.5	18.2 \pm 0.1	19.0 \pm 3.4	19.6 \pm 5.1
Total	15173 \pm 21	23.6 \pm 0.1			61 \pm 1	425 \pm 1		
<i>AW02-002b stepped heating data (23.3 mg)</i>								
200	161.6 \pm 0.5	0.44 \pm 0.01			0.18 \pm 0.01	0.67 \pm 0.03	5.2 \pm 0.6	9.2 \pm 7.8
300	1143.3 \pm 3.5	0.92 \pm 0.02			3.6 \pm 0.2	5.9 \pm 0.1	7.0 \pm 0.7	12.2 \pm 1.2
400	1135.6 \pm 3.4	0.87 \pm 0.02			5.1 \pm 0.3	16.9 \pm 0.1	8.7 \pm 0.9	11.4 \pm 1.2
500	232.8 \pm 3.5	0.26 \pm 0.02			0.8 \pm 0.1	39.8 \pm 0.2	8.9 \pm 0.9	11.8 \pm 3.8
600	51.6 \pm 3.1	0.16 \pm 0.02			0.18 \pm 0.04	34.1 \pm 0.2	10.5 \pm 2.4	16.5 \pm 4.3
800	268.0 \pm 20.4	0.439 \pm 0.003	9.3 \pm 0.4	1.1 \pm 0.1	1.0 \pm 0.1	34.4 \pm 0.2	8.3 \pm 0.9	12.8 \pm 1.4
1000	52.5 \pm 1.2	0.117 \pm 0.001	3.0 \pm 0.1	0.8 \pm 0.0	0.24 \pm 0.02	10.2 \pm 0.1	6.8 \pm 0.9	11.4 \pm 3.7
1200	644.2 \pm 3.8	0.68 \pm 0.03	11.1 \pm 0.6	1.1 \pm 0.0	2.5 \pm 0.2	27.1 \pm 0.2	4.9 \pm 0.5	5.3 \pm 0.6
1400	4167.4 \pm 20.3	6.13 \pm 0.04	64.6 \pm 1.8	5.8 \pm 0.1	22.6 \pm 1.5	113.7 \pm 0.7	5.4 \pm 0.6	10.1 \pm 1.1
1600	3965.2 \pm 14.6	6.24 \pm 0.04	169 \pm 5	18.6 \pm 0.4	14.0 \pm 0.9	69.2 \pm 0.4	16.8 \pm 1.7	22.5 \pm 2.3
Total	11822 \pm 33	16.2 \pm 0.1			50 \pm 2	352 \pm 1		

References

- Baker, T., 1998. Alteration, mineralisation, and fluid evolution at the Eloise Cu–Au deposit, Cloncurry District, Northwest Queensland, Australia. *Econ. Geol.* **93**, 1213–1236.
- Baker, T., Perkins, C., Blake, K.L., Williams, P.J., 2001. Radiogenic and stable isotope constraints on the genesis of the Eloise Cu–Au deposit, Cloncurry District, Northwest Queensland. *Econ. Geol.* **96**, 723–742.
- Ballentine, C.J., Burgess, R., Marty, B., 2002. Tracing fluid origin, transport and interaction in the crust. In: Porcelli, D., Ballentine, C.J., Wieler, R. (Eds.), *Noble Gases in Geochemistry and Cosmochemistry. Reviews in Mineralogy and Geochemistry*, vol. 47, pp. 539–614.
- Barker, C., Robinson, S.J., 1984. Thermal release of water from natural quartz. *Am. Mineralogist* **69**, 1078–1081.
- Barton, M.D., Johnson, D.A., 1996. Evaporitic-source model for igneous related Fe oxide (REE–Cu–Au–U) mineralization. *Geology* **24**, 259–262.
- Bodnar, R.J., Binns, P.R., Hall, D.L., 1989. Synthetic fluid inclusions – VI. Quantitative evaluation of the decrepitation behaviour of fluid inclusions in quartz at one atmosphere confining pressure. *J. Metamorphic Geol.* **7**, 229–242.
- Böhlke, J.K., Irwin, J.J., 1992a. Laserprobe analyses of Cl, Br, I, and K in fluid inclusions: implications for the sources of salinity in some ancient hydrothermal fluids. *Geochim. Cosmochim. Acta* **56**, 203–225.
- Böhlke, J.K., Irwin, J.J., 1992b. Brine history indicated by argon, krypton, chlorine, bromine, and iodine analyses of fluid inclusions from the Mississippi Valley type lead–fluorite–barite deposits at Hansonburg, New Mexico. *Earth Planet. Sci. Lett.* **110**, 51–66.
- Böhlke, J.K., Irwin, J.J., 1992c. Laser microprobe analyses of noble gas isotopes and halogens in fluid inclusions: analyses of microstandards and synthetic inclusions in quartz. *Geochim. Cosmochim. Acta* **56**, 187–201.
- Burnard, P., Graham, D., Turner, G., 1997. Vesicle-specific noble gas analyses of “popping rock”; implications for primordial noble gases in the Earth. *Science* **276**, 568–571.
- Fenner, C.N., 1913. Stability relations of the silica minerals. *Am. J. Sci.* **36**, 331–384.
- Gauthier, L., Hall, G., Stein, H., Schaltegger, U., 2001. The Osborne Deposit, Cloncurry District: A 1595 Ma Cu–Au Skarn Deposit. In: Williams, P.J. (Ed.), *A Hydrothermal Odyssey, Extended conference Abstracts*. James Cook University, Townsville, pp. 58–59.
- Grant, K., Gleeson, S.A., Roberts, S., 2003. The high-temperature behavior of defect hydrogen species in quartz: implications for hydrogen isotope studies. *Am. Mineralogist* **88**, 262–270.
- Götze, J., Plötze, M., Graupner, T., Hallbauer, D.K., Bray, C.J., 2004. Trace element incorporation into quartz: a combined study by ICP-MS, electron spin resonance, cathodoluminescence, capillary ion analysis, and gas chromatography. *Geochim. Cosmochim. Acta* **68**, 3741–3759.

- Heinrich, C.A., Andrew, A.S., Wilkins, R.W.T., Patterson, D.J., 1989. A fluid inclusion and stable isotope study of synmetamorphic copper ore formation at Mount Isa, Australia. *Econ. Geol.* **84**, 529–550.
- Heinrich, C.A., Bain, J.H.C., Fardy, J.J., Waring, C.L., 1993. Br/Cl geochemistry of hydrothermal brines associated with Proterozoic metasediment-hosted copper mineralisation at Mount Isa, northern Australia. *Geochim. Cosmochim. Acta* **57**, 2991–3000.
- Hummel, F.A., 1984. *Introduction to phase equilibria in ceramic systems*. Marcel Dekker, New York, pp. 400, ISBN 0824771524.
- Ihinger, P.H., Zink, S.I., 2000. Determination of relative growth rates of natural quartz crystals. *Nature* **404**, 865–869.
- Irwin, J.J., Reynolds, J.H., 1995. Multiple stages of fluid trapping in the Stripa granite indicated by laser microprobe analysis of Cl, Br, I, K, U, and nucleogenic plus radiogenic Ar, Kr and Xe in fluid inclusions. *Geochim. Cosmochim. Acta* **59**, 355–369.
- Irwin, J.J., Roedder, E., 1995. Diverse origins of fluid inclusions at Bingham (Utah, USA), Butte (Montana, USA), St. Austell (Cornwall, UK) and Ascension Island (mid-Atlantic, UK), indicated by laser microprobe analysis of Cl, K, Br, I, Ba + Te, U, Ar, Kr, and Xe. *Geochim. Cosmochim. Acta* **59** (2), 295–312.
- Ishiyama, D., Shinoda, K., Shimizu, T., Matsubaya, O., Aikawa, N., 1999. Structural states and isotopic compositions of water in hydrothermal Quartz, Koryu Deposit, Japan. *Econ. Geol.* **94**, 1347–1352.
- Johnson, L.H., Burgess, R., Turner, G., Milledge, H.J., Harris, J.W., 2000. Noble gas and halogen geochemistry of mantle fluids: Comparison of African and Canadian diamonds. *Geochim. Cosmochim. Acta* **64**, 717–732.
- Kelley, S., Turner, G., Butterfield, A.W., Shepherd, T.J., 1986. The source and significance of argon isotopes in fluid inclusions from areas of mineralisation. *Earth Planet. Sci. Lett.* **79**, 303–318.
- Kendrick, M.A., Burgess, R., Patrick, R.A.D., Turner, G., 2001a. Halogen and Ar–Ar age determinations of inclusions within quartz veins from porphyry copper deposits using complementary noble gas extraction techniques. *Chem. Geol.* **177**, 351–370.
- Kendrick, M.A., Burgess, R., Patrick, R.A.D., Turner, G., 2001b. Noble gas and halogen evidence on the origin of Cu-Porphyry mineralising fluids. *Geochim. Cosmochim. Acta* **65**, 2651–2668.
- Kendrick, M.A., Burgess, R., Patrick, R.A.D., Turner, G., 2002a. Hydrothermal fluid origins in a fluorite-rich Mississippi valley-type deposit: combined noble gas (He, Ar, Kr) and halogen (Cl, Br, I) analysis of fluid inclusions from the South Pennine Orefield, United Kingdom. *Econ. Geol.* **97** (3), 435–451.
- Kendrick, M.A., Burgess, R., Leach, D., Patrick, R.A.D., 2002b. Hydrothermal fluid origins in Mississippi valley-type ore deposits: combined noble gas (He, Ar, Kr) and halogen (Cl, Br, I) analysis of fluid inclusions from the Illinois-Kentucky Fluorspar district, Viburnum Trend, and Tri-State districts, mid-continent United States. *Econ. Geol.* **97** (3), 452–479.
- Kendrick, M.A., Burgess, R., Harrison, D., Bjørlykke, A., 2005. Noble gas and halogen evidence on the origin of Scandinavian sandstone-hosted Pb–Zn deposits. *Geochim. Cosmochim. Acta* **69**, 109–129.
- Kendrick, M.A., Phillips, D., Miller, J.McC., 2006. Part II. Evaluation of ^{40}Ar – ^{39}Ar Ar quartz ages: implications for fluid inclusion retentivity and determination of initial $^{40}\text{Ar}/^{36}\text{Ar}$ Ar values in proterozoic samples. *Geochim. Cosmochim. Acta* **70**, 2562–2576.
- Mark, G., Pollard, P.J., 2003. Contrasting composition of metasomatic and metamorphic scapolite in the Eastern Fold Belt, Northwest Queensland, Australia. In: Eliopoulos, et al. (Eds.), *Mineral Exploration and Sustainable Development*. Millpress, Rotterdam, ISBN 90 77017 77 1.
- Mark, G., Foster, D.R.W., Pollard, P.J., Williams, P.J., Tolman, J., Darvall, M., Blake, K.L., 2004. Stable isotope evidence for magmatic fluid input during large-scale Na–Ca alteration in the Cloncurry Fe oxide Cu–Au district, NW Queensland, Australia. *Terra Nova* **16**, 54–61.
- Mavrogenes, J.A., Bodnar, R.J., 1994. Hydrogen movement into and out of fluid inclusions in quartz: Experimental evidence and geologic implications. *Geochim. Cosmochim. Acta* **58**, 141–148.
- Moreira, M., Kunz, J., Allegre, C.J., 1998. Rare gas systematics in popping rock: isotopic and elemental compositions in the upper mantle. *Science* **279**, 1178–1181.
- Ozima, M., Podeseck, F.A., 2002. *Noble Gas Geochemistry*, second ed. Cambridge University Press, Cambridge UK, pp. 286.
- Pan, Y., Dong, P., 2003. Bromine in scapolite-group minerals and sodalite: XRF microprobe analysis, exchange experiments, and application to skarn deposits. *Can. Mineralogist* **41**, 529–540.
- Perkins, C., Heinrich, C.A., Wyborn, L.A.I., 1999. $^{40}\text{Ar}/^{39}\text{Ar}$ geochronology of copper mineralisation and regional alteration, Mount Isa, Australia. *Econ. Geol.* **94**, 23–36.
- Roedder, E., 1984. Fluid inclusions. *Rev. Mineral.*, 12.
- Simon, K., 2001. Does δD from fluid inclusion in quartz reflect the original hydrothermal fluid? *Chem. Geol.* **177**, 483–495.
- Sosman, R.B., 1965. *The Phases of Silica*. Rutgers University Press, New Brunswick, New Jersey, pp. 388.
- Turner, G., Bannon, M.P., 1992. Argon isotope geochemistry of inclusion fluids from granite-associated mineral veins in southwest and northeast England. *Geochim. Cosmochim. Acta* **56**, 227–243.
- Turner, G., Burnard, P., Ford, J.L., Gilmour, J.D., Lyon, I.C., Stuart, F.M., 1993. Tracing fluid sources and interactions. *Phil. Trans. Roy. Soc. Lon. A* **344**, 127–140.
- Tuttle, O.F., Bowen, N.L., 1958. Experimental studies in the system $\text{NaAlSi}_3\text{O}_8$ – KAlSi_3O_8 – SiO_2 – H_2O . *Memoir Geol. Soc. Am.* **74**, 153.
- Watson, E.B., Cherniak, D.J., 2003. Lattice diffusion of Ar in quartz, with constraints on Ar solubility and evidence of nanopores. *Geochim. Cosmochim. Acta* **67**, 2043–2062.
- Williams, P.J., 1998. Metalliferous economic geology of the Mt Isa Eastern Succession, Queensland. *Aust. J. Earth Sci.* **45**, 329–341.
- Worden, R.H., 1996. Controls on halogen concentrations in sedimentary formation waters. *Min. Mag.* **60**, 259–274.
- Zherebtsova, I.K., Volkova, N.N., 1966. Experimental study of behaviour of trace elements in the process of natural solar evaporation of Black Sea water and Lake Sasyk-Sivash brine. *Geochem. Int.* **3**, 656–670.